Title

Full title: **Kinetics of CDK4/6 inhibition determine different temporal locations of the restriction point**

Authors

Sungsoo Kim[1,*], Alessandra Leong[1,*], Chellam Nayar[1], Minah Kim[1,†] & Hee Won Yang[1,†]

Affiliations

[1]Department of Pathology and Cell Biology, Columbia University Medical Center, New York, NY, 10032, USA

[*]These authors contributed equally to this work

[†]Correspondence to: mk4242@cumc.columbia.edu, hy2602@cumc.columbia.edu

Abstract

Mitogenic and stress signaling pathways regulate CDK4/6 activity to control entry into the cell cycle until cells pass the restriction point, after which cells irreversibly commit to the cell cycle. Previous studies have proposed that positive feedback between CDK2 and Rb, and double-negative feedback between APC/C^{Cdh1} and Emi1 cause irreversible Rb hyperphosphorylation and APC/C^{Cdh1} inactivation, respectively, to trigger the restriction point. Here, we propose that CDK2-Rb feedback is the primary signaling network that regulates the restriction point with respect to both mitogenic and stress signaling. We show that CDK4/6 activity is sufficient to initiate Rb hyperphosphorylation and E2F activation, and then high CDK2 activity maintains Rb hyperphosphorylation, triggering the transition into CDK4/6-independent cell-cycle entry. While mitogen removal results in the slow inactivation of CDK4/6, induction of stress rapidly suppresses CDK4/6 activity and can reverse cell-cycle entry even after APC/C^{Cdh1} inactivation. An increase in CDK2 activity triggers CDK2-Rb feedback without involvement of other mechanisms in S phase, indicating that activity-based substrate specificity for CDK2 is the key determinant in initiating CDK2-Rb feedback. Our finding that mitogenic and stress signaling induce different temporal locations of the restriction point reveals how cells utilize a safety mechanism to differentially regulate cell-cycle entry depending on extracellular environment.

Introduction

Mammalian cells integrate extracellular mitogenic and stress signaling to determine cell-cycle entry by regulating cyclin-dependent kinase 4 and 6 (CDK4/6) activity (Arora et al., 2017; Heldt et al., 2018; Topacio et al., 2019; Yang et al., 2017). To enter the cell cycle, cells must cross the restriction point where cells irreversibly commit to the cell cycle (Pardee, 1974; Planas-Silva and Weinberg, 1997). This provides a safety mechanism to maintain genome stability by protecting against incomplete DNA replication (Henley and Dick, 2012; Matson and Cook, 2017). The restriction point was first defined in mitogen-starved cells as a point in G1 phase where cells commit to the cell cycle regardless of mitogen availability (Pardee, 1974). In cycling cells, the restriction point with respect to mitogen removal can be located in the G2-phase of mother cells (Spencer et al., 2013).

Mechanistically, the retinoblastoma (Rb)/E2F pathway is central to the regulation of the restriction point. During quiescence, Rb serves as a transcriptional co-repressor that binds E2F proteins and represses their transcriptional activities (Fisher, 2016; Matson and Cook, 2017). It is known that CDK4/6 activity partially phosphorylates Rb, then CDK2-mediated positive feedback triggers irreversible Rb hyperphosphorylation (Connell-Crowley et al., 1997; Fisher, 2016; Lundberg and Weinberg, 1998; Matson and Cook, 2017; Merrick et al., 2011; Sherr and Roberts, 1999; Weinberg, 1995). Recent findings, however, revealed that stress signaling can reverse Rb hyperphosphorylation even after CDK2 activation, challenging the canonical model (Cappell et al., 2016). Instead, the same study proposed that inactivation of the anaphase-promoting complex/cyclosome-Cdh1 (APC/C^{Cdh1}) is an irreversible and bistable switch that regulates the restriction point with respect to stress signaling (Figure 1A). Double-negative feedback between APC/C^{Cdh1} and Emi1 underlies the molecular mechanism of irreversible inactivation of APC/C^{Cdh1} (Cappell et al., 2018). These studies suggest that mitogenic and stress signaling utilize different feedback mechanisms to trigger the restriction point. Since both APC/C^{Cdh1}-Emi1 and CDK2-Rb feedbacks engage at the onset of S phase (Cappell et al., 2016; Chung et al., 2019), inactivation of CDK4/6 before the initiation of S phase can reverse cell-cycle entry. Furthermore, recent studies demonstrated that while CDK4/6 activity can be sustained after mitogen withdrawal (Chung et al., 2019), induction of stress signaling rapidly suppresses CDK4/6 activity (Yang et al., 2020), raising the possibility that temporal locations of the restriction point can be different depending on the external stimuli. Nevertheless, it remains unclear how the distinct feedbacks coordinate timing of the restriction point and S-phase entry and whether other mechanisms in S phase are required to initiate the restriction point.

Here we propose that CDK2-Rb feedback is the key signaling network regulating the restriction point with respect both mitogenic and stress signaling and the timing of S-phase entry. CDK4/6 activation initiates Rb hyperphosphorylation and subsequently induction of E2F activity. Once CDK2 activity reaches a threshold level, it sequentially activates CDK2-Rb feedback and DNA replication, controlling the transition into CDK4/6-independent cell-cycle entry and S-phase entry. Using a live-cell sensor for CDK4/6 activity (Yang et al., 2020), we show that mitogen removal resulted in the slow inactivation of CDK4/6, locating the restriction point multiple hours before engagement of CDK2-Rb feedback. On the other hand, induction of DNA damage caused rapid CDK4/6 inactivation and reversed cell-cycle entry. This indicates that the restriction point with respect to stress signaling is temporally located close to engagement of CDK2-Rb feedback. While high CDK2 activity typically triggers the CDK2-Rb pathway at the onset of S phase, an increase in CDK2 activity is sufficient to initiate CDK2-Rb feedback in G1, suggesting activity-based substrate specificity for CDK2. Our findings indicate that temporal control of the restriction point allows for cells to differentially respond to variable changes in the extracellular environment,

thus providing a safety mechanism before S-phase entry if external conditions become unfavorable for DNA replication.

Results

CDK4/6 initiates Rb hyperphosphorylation, then high CDK2 activity triggers CDK2-Rb feedback

We explored how CDK4/6 and CDK2 coordinate the Rb/E2F pathway. It has been proposed that phosphorylation of Rb by CDK4/6 is sufficient to disrupt the Rb/E2F interaction and initiate the cell cycle (Fisher, 2016; Lundberg and Weinberg, 1998; Matson and Cook, 2017; Merrick et al., 2011; Sherr and Roberts, 1999; Weinberg, 1995). However, recent studies demonstrated that CDK4/6 monophosphorylates Rb and E2F targets remain suppressed unless Rb is hyperphosphorylated by CDK2 (Narasimha et al., 2014; Sanidas et al., 2019). An additional study reported that CDK4/6 activity can induce Rb hyperphosphorylation in mouse embryonic fibroblasts (MEFs) lacking all four cyclinE1/2 and A1/2 genes (Chung et al., 2019). To clarify the regulation of the Rb/E2F pathway by CDK4/6 and CDK2, we used a live-cell reporter for CDK4/6 activity that we recently developed (Yang et al., 2020) and combined with other live-cell reporters for CDK2 (Hahn et al., 2009; Spencer et al., 2013) and APC/C^{Cdh1} (Cappell et al., 2016; Sakaue-Sawano et al., 2008) activities in human epithelial MCF-10A cells (Figure 1B). We note that the CDK2 sensor generally measures the collective activity of cyclin E/A-CDK1/2 complexes (Schwarz et al., 2018). To account for CDK2 activity in S and G2 phase that may be captured by the CDK4/6 sensor, we derived a corrected CDK4/6 activity by subtracting a calculated fraction of the CDK2 reporter signal (Yang et al., 2020). In the same cells, we performed immunostaining to measure Rb phosphorylation at S807/811, a marker for Rb hyperphosphorylation (Cappell et al., 2016; Chung et al., 2019; Yang et al., 2017), and mRNA fluorescence *in situ* hybridization (FISH) to measure the E2F target gene, E2F1 (Figure 1C, top). We synchronized cells in quiescence (G0) by mitogen starvation for 48 hours, then stimulated cells with mitogens (hereafter mitogen release) and fixed them at various time points. Based on the distributions of the CDK activities, intensity of the APC/C^{Cdh1} reporter, and Rb phosphorylation levels, we classified populations for active CDK4/6 and CDK2, inactive APC/C^{Cdh1}, and Rb phosphorylation at S807/811 (Figure 1C, bottom). When we plotted the percentages of cells in each population and the averaged E2F1 mRNA level as a function of time after mitogen stimulation, we found that CDK4/6 activation, Rb phosphorylation at S807/811, and E2F transcription activity were tightly coordinated before CDK2 activation and APC/C^{Cdh1} inactivation (Figure 1D). We note that APC/C^{Cdh1} induces cyclin A protein degradation (Sudakin et al., 1995; Zachariae and Nasmyth, 1999), therefore cyclin E-CDK1/2 activity can be measured by the CDK2 reporter before APC/C^{Cdh1} inactivation. Furthermore, at the single-cell level, CDK4/6 activation and Rb phosphorylation at S807/811 were strongly correlated, while CDK2 activity started increasing only after both Rb phosphorylation at S807/811 and onset of CDK4/6 activity (Figure S1, A and B). By analyzing three-dimensional activity maps of CDK4/6 versus CDK2 where the percentages of inactive APC/C^{Cdh1}, Rb phosphorylation at S807/811, and E2F1 mRNA levels are color-coded, we found that activation of CDK4/6 tightly correlated with Rb phosphorylation at S807/811 and increased E2F1 mRNA levels (Figure S1B). APC/C^{Cdh1} was inactivated only in the cells with both CDK4/6 and CDK2 activities (Figure S1B). Our data indicate that activation of CDK4/6 is tightly coupled with Rb phosphorylation and with the initiation of E2F activity before CDK2 activation.

We next used multiplex staining (Gut et al., 2018) to sequentially measure multiple sites of Rb phosphorylation at S807/811, T373, S608, and S780 in the same MCF-10A cells (Figure 1E). We confirmed that all Rb-phosphorylation sites measured by four different antibodies were closely correlated at the single-cell level (Figure S1C) (Chung et al., 2019). By analyzing three-dimensional activity maps of CDK4/6 versus CDK2 color-coded for the percentage of Rb phosphorylation, we

found that CDK4/6 activity is tightly coupled with four Rb phosphorylation sites at S807/811, T373, S608, and S780 (Figure 1F). Furthermore, E2F1 mRNA levels started increasing at the boundary of Rb phosphorylation at S807/811, suggesting the lower and the upper peaks of phosphorylation at S807/811 infer un-/mono- and hyper-phosphorylation of Rb, respectively (Figure 1G). We also observed similar results, that CDK4/6 activity is sufficient to trigger Rb phosphorylation at S807/811 and E2F activation in asynchronously cycling and passage-limited human lung fibroblasts (HLF) and human foreskin fibroblasts (HS68), as well as hTERT immortalized human foreskin fibroblasts (BJ-5ta) (Figure 1, H and I, and Figure S1D). These results suggest that regulation of the Rb/E2F pathway by CDK4/6 is conserved across several primary and immortalized cell types. Building on previous studies showing the hyperphosphorylated, inactive form of Rb is associated with reduced binding to the nuclear compartment (Chung et al., 2019; Mittnacht and Weinberg, 1991), we further used *in situ* extraction of soluble proteins with a low-salt buffer in MCF-10A cells to induce the loss of hyperphosphorylated Rb and the retention of nuclear-bound Rb, inferring a hypo-phosphorylated Rb state. Consistently, CDK4/6 activity was inversely correlated with nuclear-bound Rb (Figure S1E). We next classified cells into nuclear-bound Rb (hypophosphorylated) and nuclear-unbound Rb (hyperphosphorylated) populations and analyzed three-dimensional activity maps of CDK4/6 versus CDK2 where the percentage of nuclear-unbound Rb is color-coded. We found that CDK4/6 activation immediately triggered nuclear-unbound Rb (Figure 1J). Given that CDK4/6 activation induces Rb phosphorylation, our data suggest that Rb phosphorylation should be reversible by CDK4/6 inhibition, but not by CDK2 inhibition. To test this hypothesis, we used CDK4/6 inhibitors (palbociclib, abemaciclib, and ribociclib). Each of the three CDK4/6 inhibitors reversed Rb-phosphorylation at S807/811, T373, S608, and S780, while none of these sites were affected by acute treatment with CDK2 inhibitors (roscovitine and CDK2iIII) (Figure 1K and Figure S2). In addition, Rb phosphorylation is resistant to CDK4/6 inhibition in cells with high CDK2 activity, suggesting that high CDK2 activity is required to trigger CDK2-Rb feedback. Together, we propose that CDK4/6 activity is sufficient to initiate Rb phosphorylation and E2F activation, after which high CDK2 activity maintains Rb phosphorylation.

Our data also suggests that CDK2 inhibition alone is not expected to prevent Rb phosphorylation. However, previous studies showed that CDK2 inhibitors caused a loss of Rb phosphorylation and induced quiescence (Narasimha et al., 2014; Spencer et al., 2013) Therefore, we sought to understand whether these results are due to off-target effects of CDK2 inhibitors by testing the specificity of various CDK inhibitors in MCF-10A cells. To test this, cells were mitogen-released for 11 hours prior to drug treatment and CDK4/6^{high} cells with CDK2 activity (>0.6) were selected. Both the control and CDK1 inhibitor (RO-3306) treatments had almost no effect on CDK4/6 and CDK2 activities (Figure S3A). However, CDK1/2 inhibitor (CDK1/2i III) suppressed both CDK2 and CDK4/6 activities in a dose-dependent and transient manner (Figure S3B). While CDK2 inhibitors (roscovitine and CDK2i III) immediately suppressed CDK2 activity, they also slowly inhibited CDK4/6 activity, which reached close to basal levels after 9 hours of drug incubation (Figure S3C). This result is also supported by previous reports showing roscovitine suppresses RNA synthesis (Ljungman and Paulsen, 2001; MacCallum et al., 2005). All CDK4/6 inhibitors immediately blocked CDK4/6 activity (Figure S3D). Together, our data show that off-target effects of CDK1/2 and CDK2 inhibitors (Roscovitine and CDK2i III, after more than 9 hours incubation) can suppress not only CDK2 activity, but also CDK4/6 activity and thereby result in the loss of Rb phosphorylation.

CDK4/6 is sufficient to initiate full activation of E2F

To explore the kinetics of Rb phosphorylation and E2F activity with respect to CDK4/6 and CDK2 activation, we used live-cell imaging to monitor CDK4/6, CDK2, and APC/C^{Cdh1} activities and

performed fixed-cell analysis to measure Rb phosphorylation and mRNA levels of E2F target genes in MCF-10A cells. After mitogen stimulation, cells either activated CDK4/6 to initiate proliferation (CDK4/6^{high}) or maintained low CDK4/6 activity and remained in quiescence (CDK4/6^{low}) (Figure S4A) (Yang et al., 2020). CDK4/6^{high} cells consequently induced CDK2 activation, and APC/C^{Cdh1} inactivation and exhibited substantial heterogeneity in the timing of CDK4/6 activation (Figure 2A and Figure S4A), allowing us to measure Rb phosphorylation and E2F target genes at various time points after CDK4/6 activation. By mapping fixed-cell data back to live-cell data at the single-cell level, we compared Rb phosphorylation levels between CDK4/6^{high} and CDK4/6^{low} cells. Consistent with our finding that CDK4/6 activity and Rb phosphorylation are tightly coupled, all four Rb-phosphorylation sites were well correlated with CDK4/6^{high} cells (Figure S4B). When we aligned traces and fixed data by the time of CDK4/6 activation (CDK4/6-on), we found heterogeneous responses in the timing of CDK2 activation (CDK2-on) (Figure 2B and Figure S4C). Approximately 40% of CDK4/6^{high} cells did not activate CDK2 before fixation (Figure S4D). Thus, to test how CDK2 activation impacts the kinetics of Rb hyper-phosphorylation, we further classified CDK4/6^{high} cells into populations with or without CDK2 activation (Figure 2C and Figure S4, E-G). We note that while CDK4/6 activity reached the maximum level within 2 hours, CDK2 activity gradually increased (Figure 2C). When we plotted the percentage of Rb phosphorylation after CDK4/6 activation, we found that the percentage of Rb phosphorylation at S807/811, T373, S608, and S780 were almost indistinguishable in CDK4/6^{high} cells regardless of CDK2 activity, confirming our previous conclusion that CDK4/6 is sufficient to induce Rb hyperphosphorylation (Figure 2, D-G). However, when we measured E2F activity, CDK4/6^{high} cells with CDK2 activity had higher levels of E2F-target genes, E2F1, Cdc25A, and cyclin E2 mRNA and cyclin E2 protein (Figure 2H and Figure S5). These data suggest 2 possibilities, that CDK2 activity contributes to E2F activity, or that heterogeneous E2F-activity levels correlate with the CDK2 classification, as E2F-target genes activate CDK2. To test these possibilities, we manipulated CDK2 activity and measured the kinetics of E2F activity. To modulate CDK2 activity, we used cyclin E1/2 siRNA to decrease endogenous cyclin E1/2 mRNA and the dihydrofolate reductase (DHFR)-trimethoprim (TMP) protein stabilization system (Iwamoto et al., 2010) to acutely increase exogenous cyclin E1 protein. In the absence of TMP, cyclin E1 protein conjugated with the DHFR domain is continuously degraded by the proteasome. Addition of TMP rapidly stabilizes cyclin E1 protein (Figure 2I). We confirmed that knockdown and acute overexpression of cyclin E1 in CDK4/6^{high} cells delayed and accelerated CDK2 activation, respectively (Figure 2J and Figure S6, A and B). Notably, mRNA expression kinetics of E2F1 and Cdc25A after CDK4/6 activation were almost identical in CDK4/6^{high} cells regardless of CDK2 activity (Figure 2K and Figure S6, C and D). Taken together, the kinetics of Rb phosphorylation and mRNA levels of E2F target genes demonstrate that CDK4/6 activity is sufficient to induce Rb hyperphosphorylation and full E2F induction.

Different temporal locations of the restriction point with respect to mitogenic and stress signaling

To understand how CDK2-Rb and APC/C^{Cdh1}-Emi1 feedbacks coordinate the restriction point with respect to mitogenic and stress signaling, we investigated when cell-cycle entry becomes CDK4/6 independent and how mitogenic and stress signaling regulate CDK4/6 and CDK2 activities with respect to the restriction point. After mitogen release, we withdrew mitogens, applied the CDK4/6 inhibitor (palbociclib), or induced stress signaling 11 hours after mitogen release. For analysis, we selected CDK4/6^{high} cells with CDK2 activity (>0.6) at the time of inhibition. Based on CDK2 response to the treatment, we used two windows to further classify cells by path, either continuing to increase CDK2 activity for proliferation (CDK2^{inc}) or reversing CDK2 activation and entering quiescence (CDK2^{low}) (Figure 3A). Consistent with previous reports showing transient hysteresis

in CDK4/6 activity after mitogen removal (Chung et al., 2019), mitogen removal inhibited CDK4/6 activity with a 4-5 hour delay and only slightly increased the percentage of $CDK2^{low}$ cells (Figure 3, A and B). To induce stress signaling, we incubated cells with neocarzinostatin (NCS) for 10 minutes to produce exogenous DNA double-stranded breaks. Both palbociclib and NCS rapidly suppressed CDK4/6 activity and significantly increased the percentage of $CDK2^{low}$ cells (Figure 3, A and B). We also found that CDK4/6 activity was not inhibited by a pulse of NCS in $CDK2^{inc}$ cells. As $CDK2^{inc}$ cells may have already entered S phase at the time of drug treatment, it is plausible that the reduced sensitivity of CDK4/6 activity to a pulse of NCS in $CDK2^{inc}$ cells is due to the absence of p21, the key mediator of stress signaling that is degraded during S phase (*23–25*). Indeed, we found that NCS-mediated inactivation of CDK4/6 and consequent reversibility in cell-cycle entry were absent in p21 knockout cells (Figure 3B and Figure S7A). Furthermore, our data with p21 knockout cells demonstrated that the effect of palbociclib on CDK2 activity is not due to indirect effects on p21 (Guiley et al., 2019). Together, our data show how mitogenic and stress signaling differentially regulate the kinetics of CDK4/6 inhibition, creating different temporal locations of the restriction point. While most cells with low CDK2 activity cross the restriction point with respect to mitogen removal, the temporal location of the restriction point with respect to stress and CDK4/6 inhibition is closely coupled with engagement of feedback pathways.

We also noticed that APC/C^{Cdh1} inactivation was reversed by CDK4/6 inhibition in both wild type and p21 knockout cells (Figure 3A and Figure S7B). When we examined the accumulation rate of the reporter for APC/C^{Cdh1} activity (Cappell et al., 2016), it became clear that even after full inactivation of APC/C^{Cdh1}, CDK4/6 inhibition by either palbociclib or a pulse of NCS caused reactivation of APC/C^{Cdh1} and cell-cycle exit (Figure 3, C and D, and Figure S7, B and C). Our data suggest that APC/C^{Cdh1} inactivation may not directly regulate the restriction point. Recent work using fission yeast showed that CDK activity level can change substrate specificity for CDK (Swaffer et al., 2016). Additional studies in mammalian cells demonstrated that engagement of CDK2-Rb feedback is triggered at the onset of S phase (Chung et al., 2019). Therefore, we next tested whether a threshold level of CDK2, instead of APC/C^{Cdh1} inactivation, correlates with irreversible cell-cycle entry. While we confirmed that the level of CDK4/6 activity typically plateaued before CDK4/6 inhibition and was not correlated with following CDK2 activity (Figure S7, D and E), our data show that CDK2 activity at the time of CDK4/6 inhibition predicts cell-cycle entry or exit in both wild type and p21 knockout cells (Figure 3E and Figure S7F). If CDK2 activity was over 1, the level at which DNA replication has previously been reported to begin (Spencer et al., 2013), cells likely continued through cell-cycle entry regardless of CDK4/6 activity and changes in external signaling. Taken together, our data suggest that CDK2-Rb pathway is the key signaling network regulating the restriction point with respect to both mitogenic and stress signaling. Our study demonstrates that inhibition of CDK4/6 activity before threshold-based activation of CDK2-Rb feedback causes cell-cycle exit. Mitogen removal and stress induce different kinetics of CDK4/6 inhibition and consequently create corresponding locations of the restriction point.

CDK2-Rb positive feedback is the key regulator of the restriction point

Although our data suggest that APC/C^{Cdh1} inactivation may not directly regulate the restriction point, it can still contribute to CDK2 activity and consequent cell-cycle commitment by regulating cyclin A protein degradation (Sudakin et al., 1995; Zachariae and Nasmyth, 1999). Thus, we further tested how APC/C^{Cdh1} inhibition contributes to the restriction point with respect to CDK4/6 inhibition. To modulate APC/C^{Cdh1} activity, we used Cdh1 (APC/C coactivator) and Emi1 (APC/C inhibitor) siRNA to prematurely inactivate APC/C^{Cdh1} and to delay APC/C^{Cdh1} inactivation, respectively. As a control, we used cyclin E1/2 siRNA to reduce CDK2 activity. After mitogen release, we selected $CDK4/6^{high}$ cells and aligned traces by the time of CDK4/6 activation. We

observed that cells with cyclin E1/2 knockdown showed delayed CDK2 activation (Figure 4, A and B). When Cdh1 knockdown induced premature APC/C^{Cdh1} inactivation, the APC/C reporter in the Cdh1 knockdown condition showed higher basal activity compared to the control (Figure 4C). Conversely, Emi1 knockdown slowed down APC/C^{Cdh1} inactivation and consequently caused lower CDK2 activity compared to the control, as APC/C^{Cdh1} degrades cyclin A (Figure 4B). Accordingly, we selected CDK4/6^{high} cells with CDK2 activity (>0.6) and tested how many cells cross the restriction point with respect to CDK4/6 inhibition at 11 hours after mitogen release. Our data show that Emi1 knockdown increased the percentage of $CDK2^{low}$ cells to almost the same level as cyclin E1/2 knockdown (Figure 4D). However, since premature inactivation of APC/C^{Cdh1} by Cdh1 knockdown did not further increase CDK2 activity (Figure 4B), the percentage of $CDK2^{low}$ cells in the Cdh1-knockdown condition was similar to that of the control (Figure 4D).

While Emi1 knockdown increased the percentage of cells reactivating APC/C^{Cdh1} regardless of CDK4/6 inhibition, cyclin E1/2 knockdown increased the percentage of cells reactivating APC/C^{Cdh1} after CDK4/6 inhibition (Figure 4E), suggesting the CDK2 activity is the main regulator of the restriction point. To further understand whether an increase in CDK2 activity can reduce cells reactivating APC/C^{Cdh1}, we used the DHFR-TMP protein stabilization system (Iwamoto et al., 2010) to acutely increase exogenous cyclin E1 protein. After mitogen release, we added a CDK4/6 inhibitor 11 hours after mitogen stimulation with or without TMP, and selected CDK4/6^{high} cells with high CDK2 activity (>0.6). We confirmed that addition of TMP did not alter either CDK2 activity or the percentage of $CDK2^{inc}$ cells in the control condition, in which cells did not express the DHFR-cyclin E1 construct (Figure 4F and Figure S8A). As expected, increased CDK2 activity led to a higher percentage of $CDK2^{inc}$ cells (Figure 3G and Figure S8B). Intriguingly, the percentage of cells reactivating APC/C^{Cdh1} was significantly lower when we increased CDK2 activity (Figure 4H). Taken together, our data suggest that APC/C^{Cdh1} inactivation contributes to the restriction point by regulating CDK2 activity, which is the key regulator to control the restriction point.

CDK2 activity coordinates the timing of CDK4/6-indpendent cell-cycle entry and sequential DNA replication

We next determined the molecular mechanism of CDK2-mediated Rb phosphorylation. Although recent studies demonstrated that engagement of CDK2-Rb feedback correlates with the onset of S phase (Chung et al., 2019), it remains unclear whether CDK2 activity alone is enough to trigger the CDK2-Rb pathway or if other regulatory mechanisms during S phase are needed. To address this, we tested whether an increase in CDK2 activity in G1 could maintain Rb phosphorylation without CDK4/6 activity. To exclude the possibility of other contributing regulatory mechanisms during S phase, we used 5-ethynyl-20-deoxyuridine (EdU) and Hoechst staining to gate cells in G0/G1. Remarkably, during G0/G1, while control cells almost completely lost Rb phosphorylation at S807/811 following acute CDK4/6 inhibition, an increase in CDK2 activity by acute cyclin E1 overexpression significantly upregulated the percentage of Rb phosphorylation at S807/811 in MCF-10A cells (Figure 5, A and B). Furthermore, we found that an increase in CDK2 activity accelerated S-phase entry (Figure 5C), suggesting CDK2 activity is the key determinant of inducing S-phase entry. Indeed, previous reports showed that CDK2 activity facilitates the initiation and progression of DNA replication (Fisher, 2011; Krude et al., 1997; Tanaka et al., 2007). We next tested in asynchronously cycling cells whether CDK2 activity controls the timing of CDK4/6-independent cell-cycle entry and S-phase entry. When we increased CDK2 activity by addition of TMP in passage-limited human umbilical vein endothelial cells (HUVECs) expressing DHFR-cyclin E1 for 6 hours, the percentage of cells entering S phase was significantly increased (Figure 5, D and E), indicating that CDK2 activity is the limiting factor to induce S-phase entry in asynchronously cycling cells. In addition, an increase in CDK2 activity significantly rescued the reduction of Rb phosphorylation at S807/811 in G0/G1 cells by

acute CDK4/6 inhibition (Figure 5, F and G), suggesting that an increase in CDK2 activity can trigger CDK2-Rb feedback and the restriction point with respect to CDK4/6 inhibition in G1 before facilitating S phase. We observed similar results that CDK2 sequentially regulates the restriction point with respect to CDK4/6 inhibition and S-phase entry in passage-limited human melanocytes, HLF, and HS68, as well as hTERT immortalized BJ-5ta and retinal pigment epithelial (RPE1-hTERT) cells (Figure 5H and Figure S9A). These data indicate that CDK2-mediated regulation of irreversible cell-cycle entry and S-phase entry is conserved across primary and immortalized cell types. In the case of CDK2 knockout (Berthet et al., 2003; Ortega et al., 2003), it has been reported that CDK1 binds to cyclin E and compensates for the loss of CDK2 by phosphorylating CDK2 substrates (Aleem et al., 2005; Cappell et al., 2016). Taken together, our data show that high CDK2 activity alone is sufficient to determine the timing of CDK4/6-independent cell-cycle entry and the initiation of DNA replication.

Discussion

Our study shows that CDK4/6 activity alone initiates RB hyperphosphorylation and E2F activation (Figure 6A). There is possibility of limited sensitivity of the CDK2 sensor to capture low CDK2 activity. Nevertheless, our data showed low CDK2 activity assessed by the CDK2 reporter could not maintain Rb phosphorylation in response to acute CDK4/6 inhibition, which may exclude the issue of low sensitivity of the CDK2 reporter. We demonstrated that CDK2-Rb feedback is the key signaling network controlling the restriction point. As mitogen removal slowly inactivates CDK4/6, the restriction point with respect to mitogen removal is located multiple hours before activation of CDK2-Rb feedback (Figure 6B, left). However, induction of stress rapidly suppresses CDK4/6 activity and consequently, the temporal location of the restriction point with respect to stress signaling is close to the onset of the CDK2-Rb feedback pathway (Figure 6B, right). Furthermore, different respective kinetics of CDK4/6 inhibition in response to mitogen removal and stress signaling explain previous observation in asynchronously cycling cells showing different locations of the restriction point (Cappell et al., 2016; Spencer et al., 2013; Yang et al., 2017) (Figure 6C). While we confirmed that CDK2 activity needs to exceed a threshold to trigger CDK2-Rb feedback, our study shows that the CDK2-Rb pathway is the primary signaling network regulating the restriction point with respect to both mitogenic and stress signaling. Furthermore, we demonstrate that CDK2 activity alone without other mechanisms in S phase determines the temporal location of the restriction point with respect to CDK4/6 inhibition and S-phase entry, providing a safety mechanism to protect against incomplete DNA replication.

Other regulatory components such as downstream of Rb phosphorylation have been proposed as regulators of the restriction point, including positive feedback from Skp2 autoinduction (Amador et al., 2007; Carrano et al., 1999; Kossatz et al., 2004; Yung et al., 2007) and E2F autoregulation (Johnson et al., 1994; Yao et al., 2008). Although our study does not directly investigate these pathways, it is possible that they may also contribute to the restriction point by controlling CDK2 activity (Figure S9B) based on our finding showing that APC/C^{Cdh1} inactivation contributes to the restriction point by regulating CDK2 activity. Since APC/C^{Cdh1} degrades cyclin A protein, APC/C^{Cdh1} inactivation can further boost CDK2 activity and potentiate engagement of the CDK2-Rb pathway.

To understand previous reports showing that CDK2 inhibitors cause loss of Rb phosphorylation and quiescence (Narasimha et al., 2014; Spencer et al., 2013), we tested the specificity of small molecules targeting CDK activities. While we show that short term inhibition of CDK2 inhibitors (rosvocitine and CDK2i III) had immediate impact on CDK2 activity, long-term treatment of CDK2 inhibitors could also suppress CDK4/6 activity. This can be explained by previous reports showing that roscovitine inhibits RNA synthesis (Ljungman and Paulsen, 2001;

MacCallum et al., 2005). Our study also reveals that the CDK1/2 inhibitor (CDK1/2i III, >0.5 μM) effectively inhibited CDK2 activity, but it affected on CDK4/6 activity. FDA-approaved CDK4/6 inhibitors are known to be highly specific for CDK4/6 activity. Recent literature demonstrated that CDK4/6 inhibitors only bind to CDK4 monomers rather than the active tyrosine phosphorylated p21-CDK4-cyclin D1 active complex (Guiley et al., 2019). Specifically, the study proposed that CDK4/6 inhibitors cause cell-cycle arrest by releasing free p21 from CDK4-cyclin D complex. Since the CDK4/6 sensor rapidly inhibited both wild type and p21 knockout MCF-10A cells, it is possible that 1) active p21-CDK4-cyclin D1 complexes are unstable, 2) there are other mechanisms regulating CDK4/6 activation, and 3) the CDK4/6 sensor may report other activities which can be targeted by CDK4/6 inhibitors. This should be further clarified in future studies.

Our data demonstrate that CDK4/6 activation is tightly correlated with the timing of Rb phosphorylation and E2F transcription activity before CDK2 activation, also suggesting that CDK4/6 activity is sufficient to trigger Rb hyperphosphorylation. Our study indicates that Rb hyperphosphorylation is reversible until CDK2 activity reaches a threshold level that triggers CDK4/6-independent cell-cycle entry and sequential DNA replication. Furthermore, we demonstrate that different extracellular environments cause different kinetics of CDK4/6 inhibition, creating distinct timings of the restriction point. Therefore, our findings provide insights into the control system and safety mechanism for cells to 1) withdraw from cell-cycle entry depending on external conditions, and 2) protect against incomplete DNA replication.

Materials and Methods

Cell Culture

MCF-10A human mammary epithelial cells (ATCC, CRL-10317) were cultured in phenol red-free DMEM/F12 (Invitrogen) and supplemented with 5% horse serum, 20 μg/ml EGF, 10 μg/ml insulin, 500 μg/ml hydrocortisone, 100 ng/ml cholera toxin, 50 U/ml penicillin, and 50 μg/ml streptomycin. For mitogen starvation, DMEM/F12 plus 0.3% BSA w/v, 500 μg/ml hydrocortisone, and 100 ng/ml cholera toxin was used. HLF primary human lung fibroblasts (Cell Appliance, 506K-05f) were cultured in HLF Growth Medium (Cell Appliance, 516K-500) kit. Human primary epidermal melanocytes (ATCC, PCS-200-013) were culture in Dermal Cell Basal Medium (PCS-200-030). HS68 primary human foreskin fibroblasts (ATCC, CRL-1635) were cultured in DMEM (Invitrogen) plus 10% FBS, 50 U/ml penicillin, and 50 μg/ml streptomycin. HUVECs human umbilical vein endothelial cells (Lonza, C2519A) were cultured in Endothelial Cell Growth Medium (Promo Cell, C-22010) kit. BJ-5ta human foreskin fibroblasts (ATCC, CRL-4001) were cultured in DMEM (Invitrogen) plus 10% FBS, 50 U/ml penicillin, and 50 μg/ml streptomycin. RPE1-hTERT human retinal pigment epithelial cells (ATCC, CRL-4000) were cultured in DMEM:F12 (Invitrogen) plus 10% FBS and 0.01 mg/mL hygromycin B. All cell lines tested negative for mycoplasma.

Antibodies and Reagents

Palbociclib (S1116), Abemaciclib (S7158), Ribociclib (S7440), and Roscovitine (S1153) were purchased from Selleck Chemicals. CDK2i III (238803) and Neocarzinostatin (N9162) were from Sigma-Aldrich. RO-3306 (217721) was from Millipore. Anti-phosphor-Rb (Ser807/811) (8516) and anti-phosphor-Rb (S608) (2181) were purchased from Cell Signaling Technology. Anti-phosphor-Rb (S780) (558385) and anti-Rb (554136) were purchased from BD Bioscience, and anti-phophor-Rb (T373) (ab52975) was obtained from Abcam.

Constructs and stable cell lines

pLenti-DHB (a.a.994–1087)-mVenus-p2a-mCherry-Rb (a.a.886–928) and mCerulean-Geminin (a.a.1–110)-p2a-H2B-iRFP670 were described previously (Yang et al., 2020). Full sequence and constructs are available from Addgene. DHFR-cyclin E1 was cloned into a pCru5 retroviral vector. To generate stable cell lines, lentiviral and retroviral constructs were introduced into MCF-10A, HLF, melanocyte, HS68, BJ-5ta, and RPE1-hTERT cells by viral transduction.

Immunofluorescence

Cells were fixed by adding 4% paraformaldehyde at a ratio of 1:1 to culture medium (final 2% paraformaldehyde) for 15 min. Then, cells were washed three times in PBS, followed by incubation in permeabilization/blocking with 0.1% triton X-100, 10% FBS, 1% BSA, and 0.01% NaN_3 for 1 hr, and stained overnight at 4ºC with primary antibodies. Primary antibodies were visualized using a secondary antibody conjugated to Alexa Fluor-488, -568, or -647. For EdU staining, cells were treated with 10 μM EdU for 15 min, then fixed and processed with aziede-modified Alexa Fluor-647 according to manufacturer's instructions (Invitrogen, #C10269). To prevent the use of fluorophores limited by fluorescent reporters, cells were chemically bleached (Lin et al., 2015). Pre-extraction (Håland et al., 2015) and multiplexed imaging (Gut et al., 2018) were previously described.

RNA FISH

RNA *in situ* hybridization was carried out using the Affymetrix Quantigene ViewRNA ISH cell assay as specified in the user manual. Briefly, cells were plated in a 96-well glass plate (Cellvis P96-1.5H-N) that was pre-hybridized with collagen (Advanced BioMatrix, #5005-B) 1:100 in PBS overnight. At the time of fixing, cells were fixed with 4% paraformaldehyde for 15 min and dehydrated overnight using 75% EtOH. After rehydration in PBS for 10 min, the cells were permeabilized with 0.2% TX-100 for 15min RT, and then treated for probe hybridization, amplification, and labeling with Alexa Fluor 555. Cells were then incubated with Hoechst (1:10,000 in PBS) for 10 min, washed three times with PBS, and left in PBS for imaging. For the cases where immunofluorescence was to be additionally performed, after imaging the FISH signal, cells were incubated with the ViewRNA wash buffer as specified in the user manual to remove the probes and allow for measurement of other fluorophores (Alexa 488 and Alexa 647).

siRNA Transfection

siRNA was transfected using DharmaFECT 1 Transfection Reagent (Horizon, T-2001) according to the manufacturer's instructions. The following siRNAs were used: Control (Integrated DNA Technologies (IDT)), Negative Control siRNA, CCNE1 (Dharmacon, siGENOME pool), CCNE2 (Dharmacon, siGENOME pool), CDH1 (IDT, hs.Ri.FZR1.13.1-3), Emi1 (IDT, hs.Ri.FBXO5.13.1-3).

CDK4 correction based on CDK2 reporter

Based on data from CDK inhibitors and MEF lacking cyclin E1/2 and A1/2, we previously reported the contribution of CDK2 activity to the CDK4/6 reporter (Yang et al., 2020). To correct for the CDK2 contribution, we applied the correction factor described previously (Yang et al., 2020). Briefly, in the presence of CDK4/6 inhibitor, we used linear regression to calculate the contribution of CDK2 activity to the CDK4/6 reporter. CDK4/6 activity = CDK4/6 activity − 35% × CDK2 activity

Microscopy

All Images were taken on an Axio Observer 7 microscope (Zeiss) using 20X objective (0.8 N.A) with 2-by-2 pixel binning. For live-cell imaging, cells were imaged every 12 min in a humidified and 37ºC chamber in 5% CO_2. Total light exposure time was kept under 400ms for each time point.

Image Analysis

All image analyses were performed with custom Matlab scripts as previously described(Cappell et al., 2016; Yang et al., 2017). Briefly, after illumination bias correction, cells were segmented, either by using Hoechst staining (fixed-cell imaging) or H2B-iRPF670 (live-cell imaging). For DHB-mVenus and mCherry-Rb measurements, cells were segmented for their cytoplasmic regions by spatially approximating a ring with an inner radius 2 µm outside of the nuclear mask and an outer radius a maximum of 10 µm outside the nuclear mask. Regions within 10 µm of another nucleus were excluded. Regions with pixel intensities indistinguishable from background (discussed below) were also excluded. For RNA FISH measurements, cells were segmented for their whole cell regions by using an area that encompasses the nucleus and reaches out as far as 50 µm outside of the nuclear mask while preventing overlap with neighboring cells. A mask of FISH puncta was generated by top hat-filtering raw images with a circular kernel of radius 4 µm and thresholding absolute intensity. The RNA puncta parameter represents an average of the number of pixels in whole cell regions. For cell tracking, the deflection-bridging algorithm was implemented to perform tracking of cells between live-cell frames as well as between the final live-cell frame and subsequent fixed-cell image.

Code & Data availability

The code for the image analysis pipeline is available at https://github.com/scappell/Cell_tracking. Additional modified scripts and source data are available from the corresponding authors upon reasonable request.

Statistical Analysis

Statistical analyses were based on a two-sample *t*-test. The data were represented either mean ± s.d. or mean ± 95% confidence intervals and the number of replicates was indicated in respective figure legends. *P* values were indicated in respective figures. No statistical methods were used to predetermine sample size. The experiments were not randomized and the investigators were not blinded to allocation during experiments and outcome assessment.

References and Notes

1. M. Arora, J. Moser, H. Phadke, A. A. Basha, S. L. Spencer, T. Meyer, S. C. Brooks, Y. A. Wang, J. A. DeCaprio, D. M. Livingston, K. Oegema, Endogenous Replication Stress in Mother Cells Leads to Quiescence of Daughter Cells. *Cell Rep*. **19**, 1351–1364 (2017).
2. F. S. Heldt, A. R. Barr, S. Cooper, C. Bakal, B. Novák, A comprehensive model for the proliferation–quiescence decision in response to endogenous DNA damage in human cells. *Proc. Natl. Acad. Sci*. **115**, 2532–2537 (2018).
3. H. W. Yang, M. Chung, T. Kudo, T. Meyer, Competing memories of mitogen and p53 signalling control cell-cycle entry. *Nature*. **549**, 404–408 (2017).
4. B. R. Topacio, E. Zatulovskiy, S. Cristea, S. Xie, C. S. Tambo, S. M. Rubin, J. Sage, M. Kõivomägi, J. M. Skotheim, Cyclin D-Cdk4,6 Drives Cell-Cycle Progression via the Retinoblastoma Protein's C-Terminal Helix. *Mol. Cell*. **74**, 758-770.e4 (2019).
5. A. B. Pardee, A restriction point for control of normal animal cell proliferation. *Proc. Natl. Acad. Sci. U. S. A*. **71**, 1286–90 (1974).
6. M. D. Planas-Silva, R. A. Weinberg, The restriction point and control of cell proliferation. *Curr. Opin. Cell Biol*. **9**, 768–772 (1997).

7. S. A. Henley, F. A. Dick, The retinoblastoma family of proteins and their regulatory functions in the mammalian cell division cycle. *Cell Div*. **7**, 10 (2012).

8. J. P. Matson, J. G. Cook, Cell cycle proliferation decisions: the impact of single cell analyses. *FEBS J*. **284**, 362–375 (2017).

9. S. L. Spencer, S. D. Cappell, F. C. Tsai, K. W. Overton, C. L. Wang, T. Meyer, The proliferation-quiescence decision is controlled by a bifurcation in CDK2 activity at mitotic exit. *Cell*. **155**, 369–383 (2013).

10. R. P. Fisher, Getting to S: CDK functions and targets on the path to cell-cycle commitment. *F1000Research*. **5**, 2374 (2016).

11. R. A. Weinberg, The retinoblastoma protein and cell cycle control. *Cell*. **81**, 323–30 (1995).

12. C. J. Sherr, J. M. Roberts, CDK inhibitors: positive and negative regulators of G1-phase progression. *Genes Dev*. **13**, 1501–12 (1999).

13. K. a. Merrick, L. Wohlbold, C. Zhang, J. J. Allen, D. Horiuchi, N. E. Huskey, A. Goga, K. M. Shokat, R. P. Fisher, Switching Cdk2 On or Off with Small Molecules to Reveal Requirements in Human Cell Proliferation. *Mol. Cell*. **42**, 624–636 (2011).

14. A. S. Lundberg, R. A. Weinberg, Functional inactivation of the retinoblastoma protein requires sequential modification by at least two distinct cyclin-cdk complexes. *Mol. Cell. Biol*. **18**, 753–61 (1998).

15. L. Connell-Crowley, J. W. Harper, D. W. Goodrich, Cyclin D1/Cdk4 regulates retinoblastoma protein-mediated cell cycle arrest by site-specific phosphorylation. *Mol. Biol. Cell*. **8**, 287–301 (1997).

16. S. D. Cappell, M. Chung, A. Jaimovich, S. L. Spencer, T. Meyer, Irreversible APCCdh1 Inactivation Underlies the Point of No Return for Cell-Cycle Entry. *Cell*. **166**, 167–180 (2016).

17. S. D. Cappell, K. G. Mark, D. Garbett, L. R. Pack, M. Rape, T. Meyer, EMI1 switches from being a substrate to an inhibitor of APC/CCDH1 to start the cell cycle. *Nature*. **558**, 313–317 (2018).

18. M. Chung, C. Liu, H. W. Yang, M. S. Köberlin, S. D. Cappell, T. Meyer, Transient Hysteresis in CDK4/6 Activity Underlies Passage of the Restriction Point in G1. Mol. *Cell*. **76**, 562–573 (2019).

19. H. W. Yang, S. D. Cappell, A. Jaimovich, C. Liu, M. Chung, L. H. Daigh, L. R. Pack, Y. Fan, S. Regot, M. Covert, T. Meyer, Stress-mediated exit to quiescence restricted by increasing persistence in CDK4/6 activation. *Elife*. **9** (2020), doi:10.7554/eLife.44571.

20. A. T. Hahn, J. T. Jones, T. Meyer, Quantitative analysis of cell cycle phase durations and PC12 differentiation using fluorescent biosensors. *Cell Cycle*. **8**, 1044–52 (2009).

21. A. Sakaue-Sawano, H. Kurokawa, T. Morimura, A. Hanyu, H. Hama, H. Osawa, S. Kashiwagi, K. Fukami, T. Miyata, H. Miyoshi, T. Imamura, M. Ogawa, H. Masai, A. Miyawaki, Visualizing Spatiotemporal Dynamics of Multicellular Cell-Cycle Progression. *Cell*. **132**, 487–498 (2008).

22. C. Schwarz, A. Johnson, M. Kõivomägi, E. Zatulovskiy, C. J. Kravitz, A. Doncic, J. M. Skotheim, A Precise Cdk Activity Threshold Determines Passage through the Restriction Point. *Mol. Cell*. **69**, 253-264.e5 (2018).

23. F. Bunz, Requirement for p53 and p21 to Sustain G2 Arrest After DNA Damage. *Science*. **282**, 1497–1501 (1998).

24. L. Krenning, F. M. Feringa, I. A. Shaltiel, J. van den Berg, R. H. Medema, Transient Activation of p53 in G2 Phase Is Sufficient to Induce Senescence. *Mol. Cell*. **55**, 59–72 (2014).

25. T. Abbas, U. Sivaprasad, K. Terai, V. Amador, M. Pagano, A. Dutta, PCNA-dependent regulation of p21 ubiquitylation and degradation via the CRL4Cdt2 ubiquitin ligase complex. *Genes Dev*. **22**, 2496–2506 (2008).

26. K. Z. Guiley, J. W. Stevenson, K. Lou, K. J. Barkovich, V. Kumarasamy, T. U. Wijeratne, K. L. Bunch, S. Tripathi, E. S. Knudsen, A. K. Witkiewicz, K. M. Shokat, S. M. Rubin, P27 allosterically activates cyclin-dependent kinase 4 and antagonizes palbociclib inhibition. *Science*. **366**, eaaw2106 (2019).

27. M. P. Swaffer, A. W. Jones, H. R. Flynn, A. P. Snijders, P. Nurse, CDK Substrate Phosphorylation and Ordering the Cell Cycle. *Cell*. **167**, 1750-1761.e16 (2016).

28. A. M. Narasimha, M. Kaulich, G. S. Shapiro, Y. J. Choi, P. Sicinski, S. F. Dowdy, Cyclin D activates the Rb tumor suppressor by mono-phosphorylation. *Elife*. **2014**, 1–21 (2014).

29. I. Sanidas, R. Morris, K. A. Fella, P. H. Rumde, M. Boukhali, E. C. Tai, D. T. Ting, M. S. Lawrence, W. Haas, N. J. Dyson, A Code of Mono-phosphorylation Modulates the Function of RB. *Mol. Cell*. **73**, 985-1000.e6 (2019).

30. V. Sudakin, D. Ganoth, A. Dahan, H. Heller, J. Hershko, F. C. Luca, J. V. Ruderman, A. Hershko, The cyclosome, a large complex containing cyclin-selective ubiquitin ligase activity, targets cyclins for destruction at the end of mitosis. *Mol. Biol. Cell*. **6**, 185–198 (1995).

31. W. Zachariae, K. Nasmyth, Whose end is destruction: Cell division and the anaphase-promoting complex. *Genes Dev*. **13** (1999), pp. 2039–2058.

32. G. Gut, M. D. Herrmann, L. Pelkmans, Multiplexed protein maps link subcellular organization to cellular states. *Science*. **361**, eaar7042 (2018).

33. S. Mittnacht, R. A. Weinberg, G1/S phosphorylation of the retinoblastoma protein is associated with an altered affinity for the nuclear compartment. *Cell*. **65**, 381–393 (1991).

34. D. E. MacCallum, J. Melville, S. Frame, K. Watt, S. Anderson, A. Gianella-Borradori, D. P. Lane, S. R. Green, Seliciclib (CYC202, R-Roscovitine) induces cell death in multiple myeloma cells by inhibition of RNA polymerase II-dependent transcription and down-regulation of Mcl-1. *Cancer Res*. **65**, 5399–5407 (2005).

35. M. Ljungman, M. T. Paulsen, The cyclin-dependent kinase inhibitor roscovitine inhibits RNA synthesis and triggers nuclear accumulation of p53 that is unmodified at Ser15 and Lys382. *Mol. Pharmacol*. **60**, 785–789 (2001).

36. M. Iwamoto, T. Björklund, C. Lundberg, D. Kirik, T. J. Wandless, A General Chemical Method to Regulate Protein Stability in the Mammalian Central Nervous System. *Chem. Biol.* **17**, 981–988 (2010).

37. T. Krude, M. Jackman, J. Pines, R. A. Laskey, Cyclin/Cdk-dependent initiation of DNA replication in a human cell-free system. *Cell*. **88**, 109–19 (1997).

38. S. Tanaka, Y.-S. Tak, H. Araki, The role of CDK in the initiation step of DNA replication in eukaryotes. *Cell Div*. **2**, 16 (2007).

39. D. Fisher, Control of DNA replication by cyclin-dependent kinases in development. *Results Probl. Cell Differ*. **53**, 201–17 (2011).

40. C. Berthet, E. Aleem, V. Coppola, L. Tessarollo, P. Kaldis, Cdk2 Knockout Mice Are Viable. *Curr. Biol*. **13**, 1775–1785 (2003).

41. S. Ortega, I. Prieto, J. Odajima, A. Martín, P. Dubus, R. Sotillo, J. L. Barbero, M. Malumbres, M. Barbacid, Cyclin-dependent kinase 2 is essential for meiosis but not for mitotic cell division in mice. *Nat. Genet*. **35**, 25–31 (2003).

42. E. Aleem, H. Kiyokawa, P. Kaldis, Cdc2–cyclin E complexes regulate the G1/S phase transition. *Nat. Cell Biol*. **7**, 831–836 (2005).

43. Y. Yung, J. L. Walker, J. M. Roberts, R. K. Assoian, A Skp2 autoinduction loop and restriction point control. *J. Cell Biol*. **178**, 741–7 (2007).

44. V. Amador, S. Ge, P. G. Santamaría, D. Guardavaccaro, M. Pagano, APC/C(Cdc20) controls the ubiquitin-mediated degradation of p21 in prometaphase. *Mol. Cell*. **27**, 462–73 (2007).

45. A. C. Carrano, E. Eytan, A. Hershko, M. Pagano, SKP2 is required for ubiquitin-mediated degradation of the CDK inhibitor p27. *Nat. Cell Biol*. **1**, 193–9 (1999).

46. U. Kossatz, N. Dietrich, L. Zender, J. Buer, M. P. Manns, N. P. Malek, Skp2-dependent degradation of p27kip1 is essential for cell cycle progression. *Genes Dev*. **18**, 2602–7 (2004).

47. G. Yao, T. J. Lee, S. Mori, J. R. Nevins, L. You, A bistable Rb–E2F switch underlies the restriction point. *Nat. Cell Biol*. **10**, 476–482 (2008).

48. D. G. Johnson, K. Ohtani, J. R. Nevins, Autoregulatory control of E2F1 expression in response to positive and negative regulators of cell cycle progression. *Genes Dev*. **8**, 1514–1525 (1994).

49. J.-R. Lin, M. Fallahi-Sichani, P. K. Sorger, Highly multiplexed imaging of single cells using a high-throughput cyclic immunofluorescence method. *Nat. Commun*. **6**, 8390 (2015).

50. T. W. Håland, E. Boye, T. Stokke, B. Grallert, R. G. Syljuåsen, Simultaneous measurement of passage through the restriction point and MCM loading in single cells. *Nucleic Acids Res*. **43**, e150 (2015).

Acknowledgments

We thank Nalin Ratnayeke for a pre-extraction protocol; Mingyu Chung for helpful comments; Tobias Meyer for helpful discussion and support; Richard Baer, Michele Pagano, and Charles Sherr for helpful discussions and critical comments. **Funding:** This work was supported by the Neuroendocrine Tumor Research Foundation (M.K., 653132) and Herbert Irving Comprehensive Cancer Center (H.Y., P30 CA013696). **Author contributions:** H.Y. conceived and conceptualized idea and H.Y., M.K., S.K., and A.L designed the research and H.Y., S.K., C.N., and A.L. performed experiments. H.Y. and M.K. interpreted and visualized the data and wrote the manuscript discussed with all authors. H.Y. and M.K. supervised the project. **Competing interests:** There are no competing interests. **Data and materials availability:** All data needed to evaluate the conclusions in the paper are present in the paper and/or the Supplementary Materials. Additional data related to this paper may be requested from the authors.

Figures

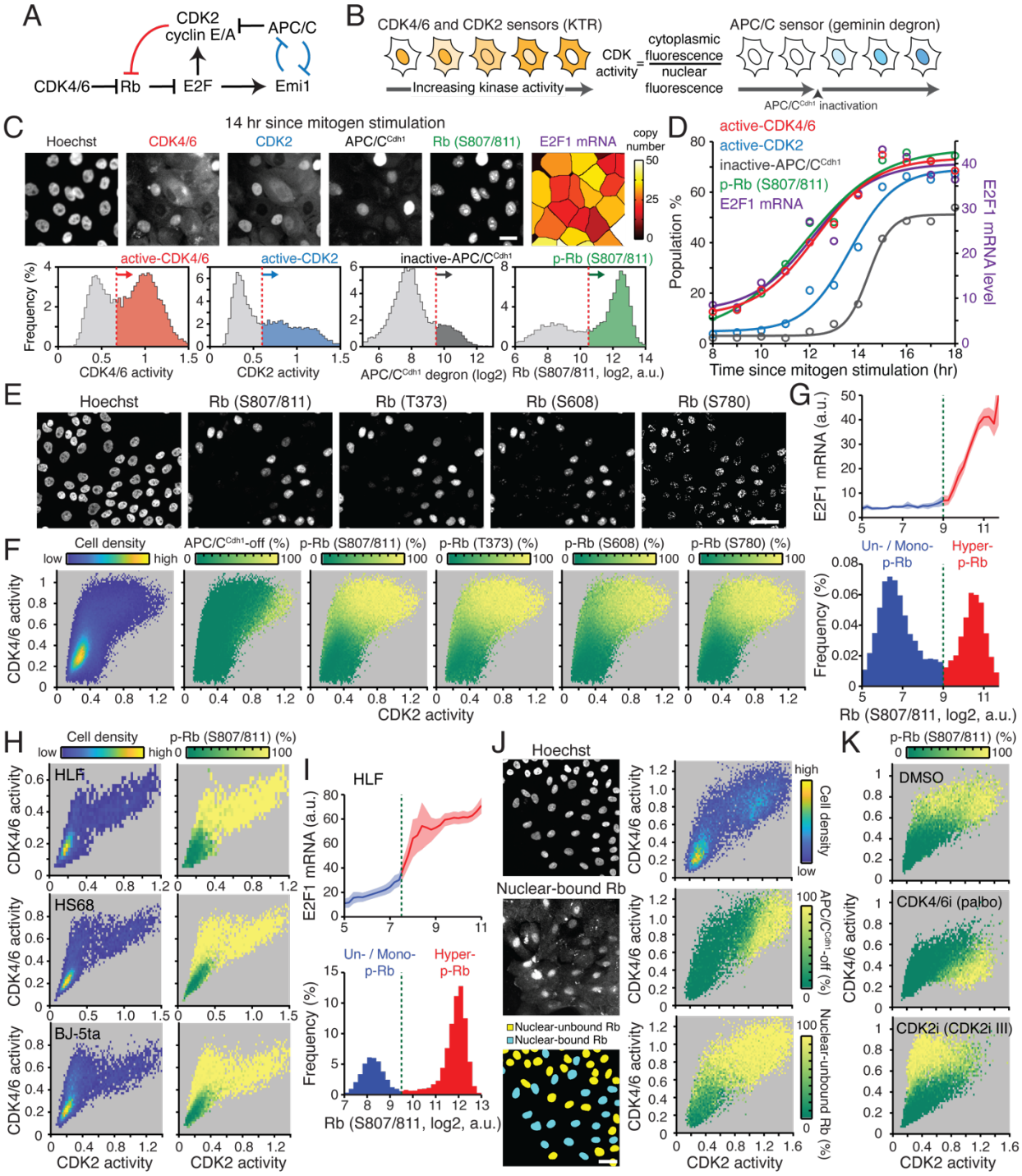

Figure 1. CDK4/6 is sufficient to induce Rb phosphorylation before high CDK2 activity level triggers CDK2-Rb feedback.

(A) Schematic of the current proposed model for regulation of the Rb/E2F pathway and cell-cycle commitment. **(B)** Schematics of CDK4/6, CDK2 reporters (left) and APC/C^{Cdh1} reporter (right). Active CDK4/6 and CDK2 phosphorylate and induce translocation of reporters to the cytoplasm. As APC/C^{cdh1} is inactivated, intensity of the reporter starts increasing. **(C)** Top, representative images of CDK4/6, CDK2, and APC/C^{Cdh1} reporters, Rb (S807/811) immunostaining, and mRNA FISH for E2F1 mRNA in the same MCF-10A cells. Scale bar is 20 µm. Bottom, histograms of CDK4/6, CDK2, and APC/C^{Cdh1} activities and phosphorylated Rb (p-Rb) at S807/811. Red dotted

line indicates a threshold used to classify active CDK4/6 and CDK2, inactive APC/C^{Cdh1}, and p-Rb populations. Cells were mitogen-released for 14 hr prior to fixation. **(D)** Scatterplot of the percent of cells with active CDK4/6, active CDK2, inactive APC/C^{Cdh1}, and p-Rb at S807/811 in MCF-10A cells as a function of time since mitogen stimulation. E2F1 mRNA level reflects averaged value over time. Solid line is sigmoidal best-fit line. **(E)** Representative images of multiplexed staining of Rb (S807/811, T373, S608, S780) in MCF-10A cells. Scale bar is 20 µm. **(F)** Three-dimensional activity map of CDK4/6 versus CDK2 activity where cell density, the percentage of inactivated APC/C^{Cdh1}, and the percentage of p-Rb at sites S807/811, T373, S608, and S780 are color-coded. MCF-10A cells were mitogen-released for 12 hr prior to fixation. **(G)** Top, E2F1 mRNA levels across the distribution of p-Rb at S807/811 in MCF-10A cells. Data are mean ± 95% confidence intervals (n = 11,741 cells). Bottom, histogram of p-Rb at S807/811. Blue and red correspond to un-/mono- and hyper-phosphorylation of Rb, respectively. **(H)** Three-dimensional activity map of CDK4/6 versus CDK2 activity in HLF, HS68, and BJ-5ta cells (top to bottom). Cell density and the percentage of p-Rb at S807/811 are color-coded. **(I)** Top, E2F1 mRNA levels across the distribution of p-Rb at S807/811 in HLF cells. Data are mean ± 95% confidence intervals (n = 18,861 cells). Bottom, histogram of p-Rb at S807/811. Blue and red correspond to un-/mono- and hyper-phosphorylation of Rb, respectively. **(J)** Left, representative images of nuclear-bound Rb after *in situ* extraction and classification of nuclear-bound and nuclear-unbound Rb. Scale bar is 20 µm. Right, three-dimensional activity maps of CDK4/6 versus CDK2 with corresponding cell density, the percentage of inactivated APC/C^{Cdh1}, and the percentage of nuclear-unbound Rb color-coded (top to bottom). MCF-10A cells were mitogen-released for 12 hr prior to *in situ* extraction. **(K)** Three-dimensional activity maps of CDK4/6 versus CDK2 activity under the control condition, CDK4/6 inhibition, and CDK2 inhibition (top to bottom). The percentage of p-Rb at S807/811 are color-coded. After mitogen release for 12 hr, MCF-10A cells were treated with Palbociclib (1 µM) or CDK2i III (60 µM) for 1 hr prior to fixation.

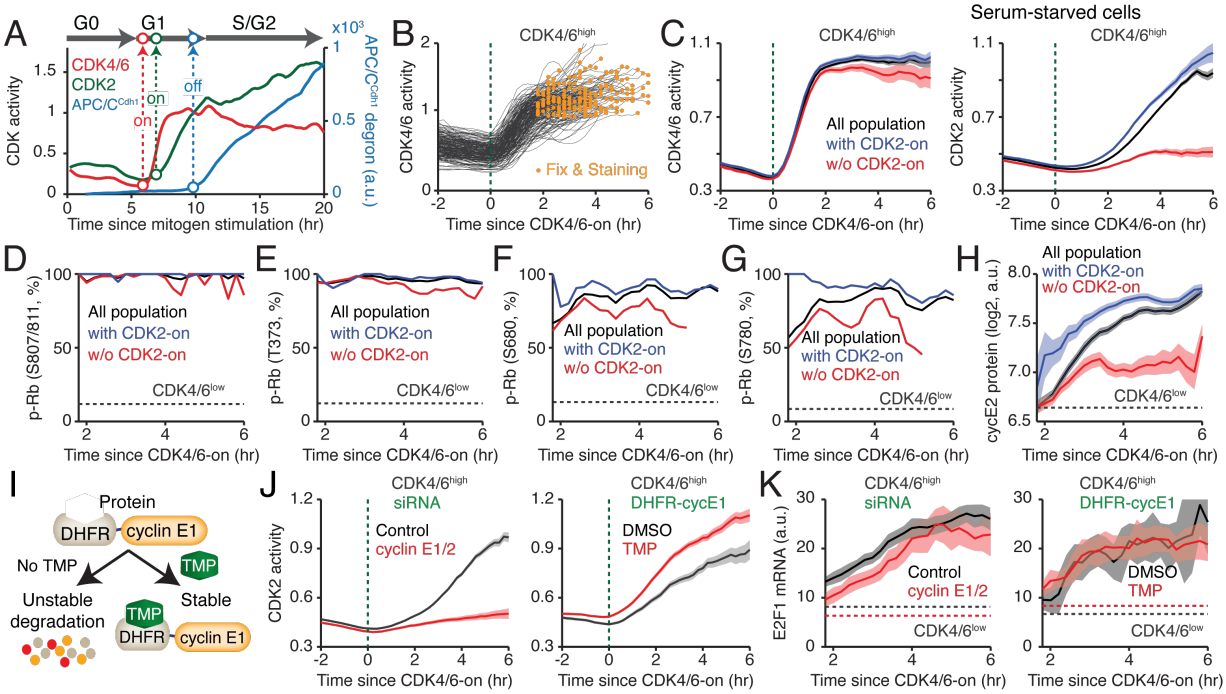

Figure 2. CDK4/6 activation triggers immediate Rb hyper-phosphorylation.
(A) Representative time course analysis of CDK4/6 activity, CDK2 activity, and APC/C^{Cdh1} inactivation labeled with cell-cycle phase and demarcation of activity/inactivity point. **(B)** Single-cell traces of CDK4/6 activity aligned to the time of CDK4/6 activation in CDK4/6^{high} cells. To create more heterogeneity, MCF-10A cells were mitogen-released for various durations (9, 10, and 11 hr) prior to fixation. Orange points correspond to fixation point. Green dotted line indicates CDK4/6 activity onset. **c,** Averaged CDK4/6 activity traces (left) and CDK2 activity traces (right) aligned to CDK4/6 activation in MCF-10A cells. Black, blue, and red lines correspond to all cells, cells with CDK2 activity, and without CDK2 activity, respectively. Green dotted line indicates CDK4/6 activity onset. Data are mean ± 95% confidence interval (All population, n=1,917 cells; with CDK2 activity, n=879 cells; w/o CDK2 activity, n=1,038 cells). **(D-G)** Percentage of p-Rb at sites S807/811 **(D)**, T373 **(E)**, S680 **(F)**, and S780 **(G)**, as a function of CDK4/6 activation in MCF-10A cells. Dotted line indicates percentage of p-Rb in CDK4/6^{low} cells. Black, blue, and red lines correspond to all cells, cells with CDK2 activity, and without CDK2 activity, respectively. **(D)** All population, n=1,917 cells; with CDK2 activity, n=1,038 cells; w/o CDK2 activity, n=879 cells; CDK4/6^{low} cells, n= 4,127 cells. **(E)** All population, n=825 cells; with CDK2 activity, n=545 cells; w/o CDK2 activity, n=280 cells; CDK4/6^{low} cells, n= 2,333 cells. **(F,G)** All population, n=494 cells; with CDK2 activity, n=332 cells; w/o CDK2 activity, n=162 cells; CDK4/6^{low} cells, n= 1,253 cells. **(H)** Averaged cyclin E2 protein levels aligned to CDK4/6 activation in MCF-10A cells. Black, blue, and red lines correspond to all cells, cells with CDK2 activity, and without CDK2 activity, respectively. Dotted line indicates cyclin E2 protein level in CDK4/6^{low} cells. Data are mean ± 95% confidence interval (All population, n=1,930 cells; with CDK2 activity, n=1,226 cells; w/o CDK2 activity, n=704 cells; CDK4/6^{low} cells, n= 3,986 cells). **(I)** Schematic of TMP-induced rapid expression of cyclin E1. **(J)** Averaged CDK2 activity traces aligned to the time of CDK4/6 activation for CDK4/6^{high} cells. Green dotted line indicates CDK4/6 activity onset. Data are mean ± 95% confidence interval (siRNA: Control, n=3,172 cells; cyclin E1/2, n=1,042 cells; DHFR-cyclin E1: DMSO, n=470 cells; TMP, n=932 cells). **(K)** Averaged E2F1 mRNA levels aligned to the time of CDK4/6 activation for CDK4/6^{high} cells. Dotted lines indicate E2F1 mRNA level in CDK4/6^{low} cells for each treatment. Data are mean ± 95% confidence interval (siRNA: Control, n=1,699 cells; cyclin E1/2, n=644 cells; DHFR-cyclin E1: DMSO, n=233 cells; TMP, n=552 cells). **(J,K)** Left, MCF-10A cells were transfected with control (black) or cyclin E1/2 (red) siRNA and

25 were mitogen-released for various durations (9, 10, and 11 hr) prior to fixation. Right, MCF-10A
26 cells expressing DHFR-cyclin E1 were mitogen-released for various durations (9, 10, and 11 hr)
27 with DMSO (black) or TMP (50 μM, red) prior to fixation.

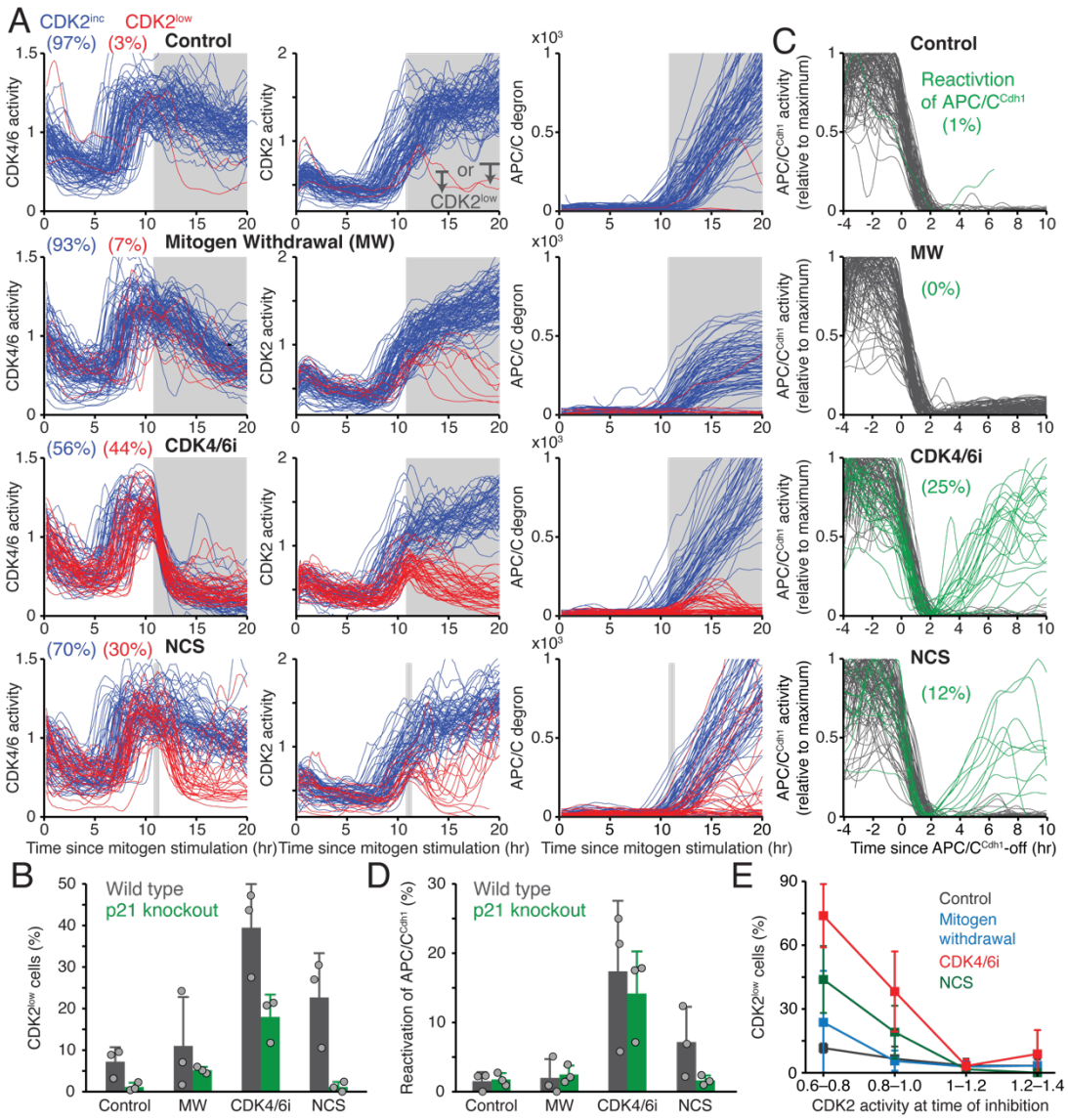

Figure 3. Kinetics of CDK4/6 inhibition by mitogen removal and stress induction determine different temporal locations of the restriction point.

(A) Single-cell traces of CDK4/6 activity (left), CDK2 activity (middle), and APC/C degron (right) in MCF-10A cells. Top to bottom, corresponding conditions under control, mitogen withdrawal, CDK4/6 inhibitor (palbociclib, 1 μM), and 10 min NCS pulse (100 ng/ml). All treatments performed at 11 hr (marked in gray). Blue and red lines correspond to $CDK2^{inc}$ and $CDK2^{low}$ cells, respectively. Cells were classified based on CDK2 activity after 4 and 9 hr of inhibition. **(B)** Percentage of $CDK2^{low}$ cells in wild type (gray) and p21 knockout (green) MCF-10A cells for each treatment condition in **(A)**. Data are mean ± s.d. (n = 3 biological replicates). **(C)** Single-cell traces of APC/C^{Cdh1} activity aligned to the time of APC/C^{Cdh1} inactivation in MCF-10A cells. Green line corresponds to cells reactivating APC/C^{Cdh1}. **(D)** Percentage of cells reactivating APC/C^{Cdh1} in wild type (gray) and p21 knockout (green) MCF-10A cells for each treatment condition in **(A)**. Data are mean ± s.d. (n = 3 biological replicates). **(E)** Percentage of $CDK2^{low}$ cells for increasing levels of CDK2 activity at the time of inhibition, in wild type MCF-10A cells. Cells were classified based on each treatment condition in **(A)** Data are mean ± s.d. (n = 3 biological replicates).

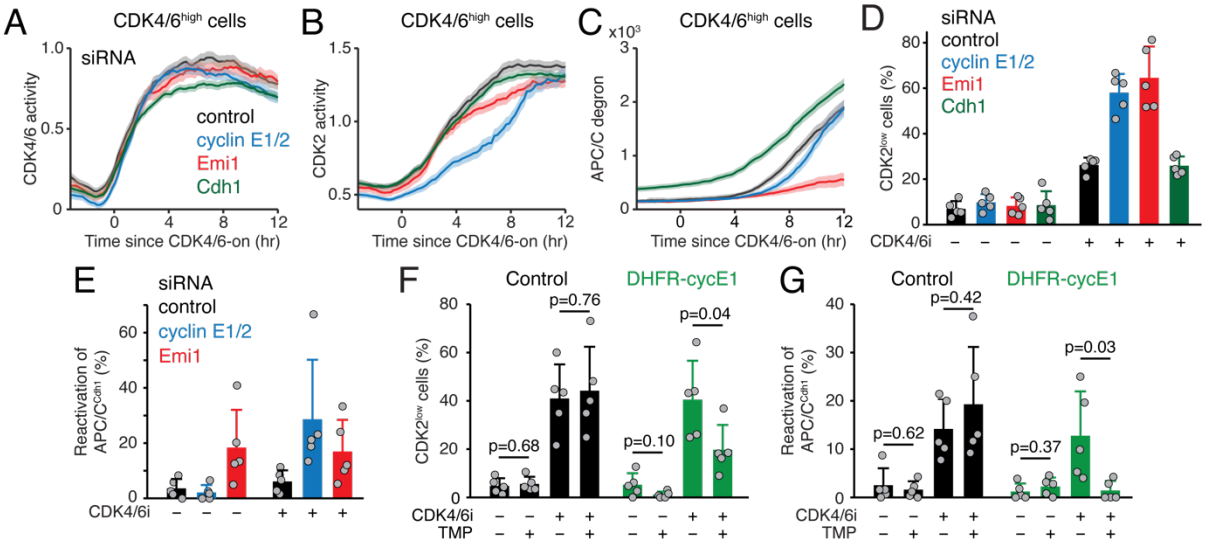

Figure 4. CDK2 activity is the key regulator of the restriction point.
(A–C), Averaged CDK4/6 activity **(A)**, CDK2 activity **(B)**, and APC/C degron **(C)** traces aligned to time of CDK4/6 activation for CDK4/6^{high} MCF-10A cells treated with control (black), cyclin E1/2 (blue), Emi1 (red), and Cdh1 (green) siRNA. Data are mean ± 95% confidence intervals (n> 200 cells for each condition) **(D, E)** Percentage of CDK2^{low} cells **(D)** and APC/C^{cdh1} reactivating cells **(E)** for each knockdown condition as indicated in MCF-10A cells without and with CDK4/6 inhibitor (palbociclib, 1 µM). Data are mean ± s.d. (n = 5 biological replicates). **(F, G)** Percentage of CDK2^{low} cells **(F)** and APC/C^{cdh1} reactivating cells **(G)** for each treatment condition as indicated in MCF-10A cells without (black) and with (green) DHFR-cyclin E1 expression. Data are mean ± s.d. (n = 5 biological replicates). P-values were calculated with two-sample t-tests.

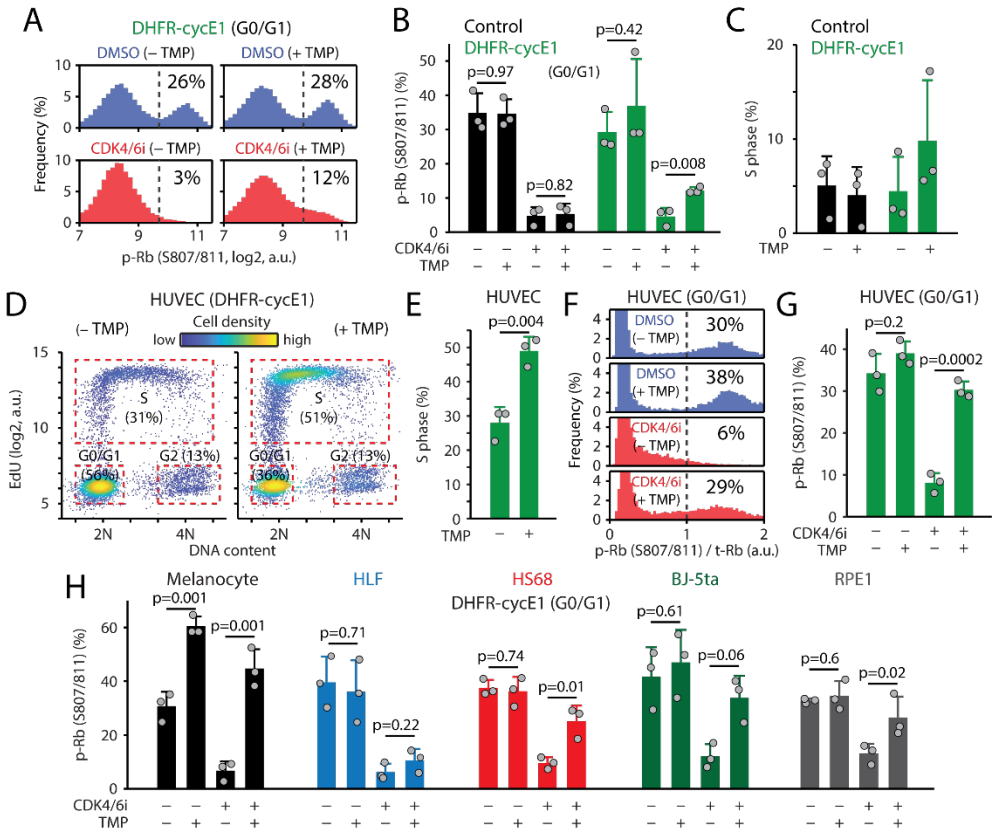

Figure 5. CDK2 activity level controls the location of the restriction point and S-phase entry. **(A, B)** Histogram of p-Rb at S807/811 for MCF-10A cells with DHFR-cyclin E1 expression in G0/G1 phase **(A)**. Percentage of p-Rb at S807/811 for each treatment condition as indicated for MCF-10A cells without (black) and with (green) DHFR-cyclin E1 expression **(B)**. Data are mean ± s.d. (n = 3 biological replicates). MCF-10A cells were mitogen-released for 11 hr with or without TMP (50 μM) followed by acute treatment with CDK4/6 inhibitor (palbociclib, 1 μM) and EdU (10 μM) for 15 min prior to fixation. P-values were calculated with two-sample t-tests. **(C)** Percentage of cells in S phase for each treatment condition indicated. MCF-10A cells without (black) and with (green) DHFR-cyclin E1 were mitogen-released with or without TMP (50 μM) for 6 hr followed by acute treatment with CDK4/6 inhibitor (palbociclib, 1 μM) and EdU (10 μM) for 15 min, prior to fixation. Data are mean ± s.d. (n = 3 biological replicates). **(D)** Scatterplot of Hoechst versus EdU, where cell density is color-coded. Cycling HUVEC cells expressing DHFR-cyclin E1 were treated with or without TMP (50 μM) for 6 hr followed by EdU (10 μM) treatment for 15 min prior to fixing and staining with Hoechst. **(E)** Percentage of cells in S phase for cycling HUVEC cells expressing DHFR-cycE1 with or without TMP (50 μM) treatment for 6 hr. Data are mean ± s.d. (n = 3 biological replicates). P-values were calculated with two-sample t-tests. **(F-H)** Histogram of p-Rb at S807/811 for HUVECs in G0/G1 phase **(F)**. Percentage of p-Rb at S807/811 for each treatment condition as indicated for HUVECs **(G)** and Melanocyte, HLF, HS68, BJ-5ta, and RPE1 cells **(H)** expressing DHFR-cyclin E1. Data are mean ± s.d. (n = 3 biological replicates). Cycling cells were treated with or without TMP (50 μM) for 6 hr followed by acute treatment with CDK4/6 inhibitor (palbociclib, 1 μM) and EdU (10 μM) for 15 min prior to fixation. P-values were calculated with two-sample t-tests.

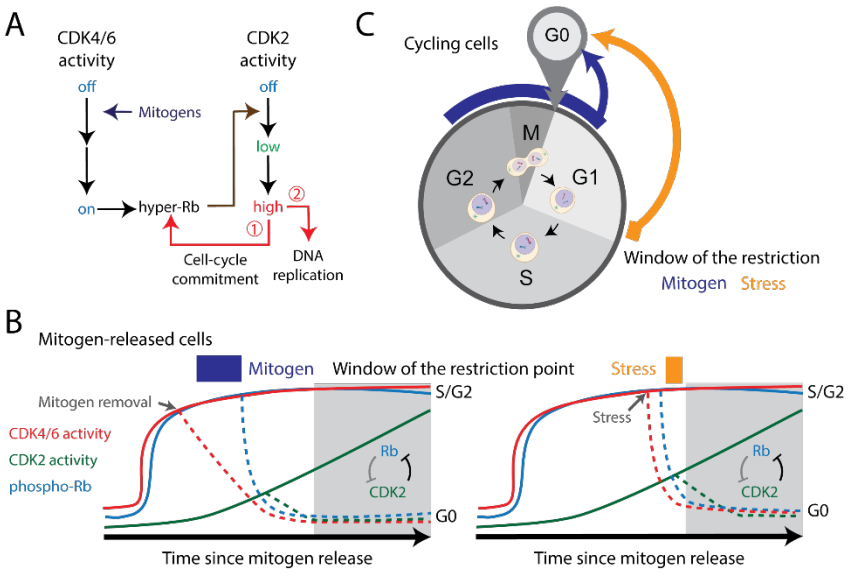

Figure 6. Models for the window of the restriction points

(A) Schematic of sequential regulation of the Rb/E2F pathway by CDK4/6 and CDK2. High CDK2 activity triggers the commitment point by maintaining Rb hyperphosphorylation, which then initiates DNA replication. **(B, C)** Schematic of two different windows of the restriction point for mitogen and stress signaling in either mitogen-released **(B)** or cycling **(C)** cells.

Supplementary Figures

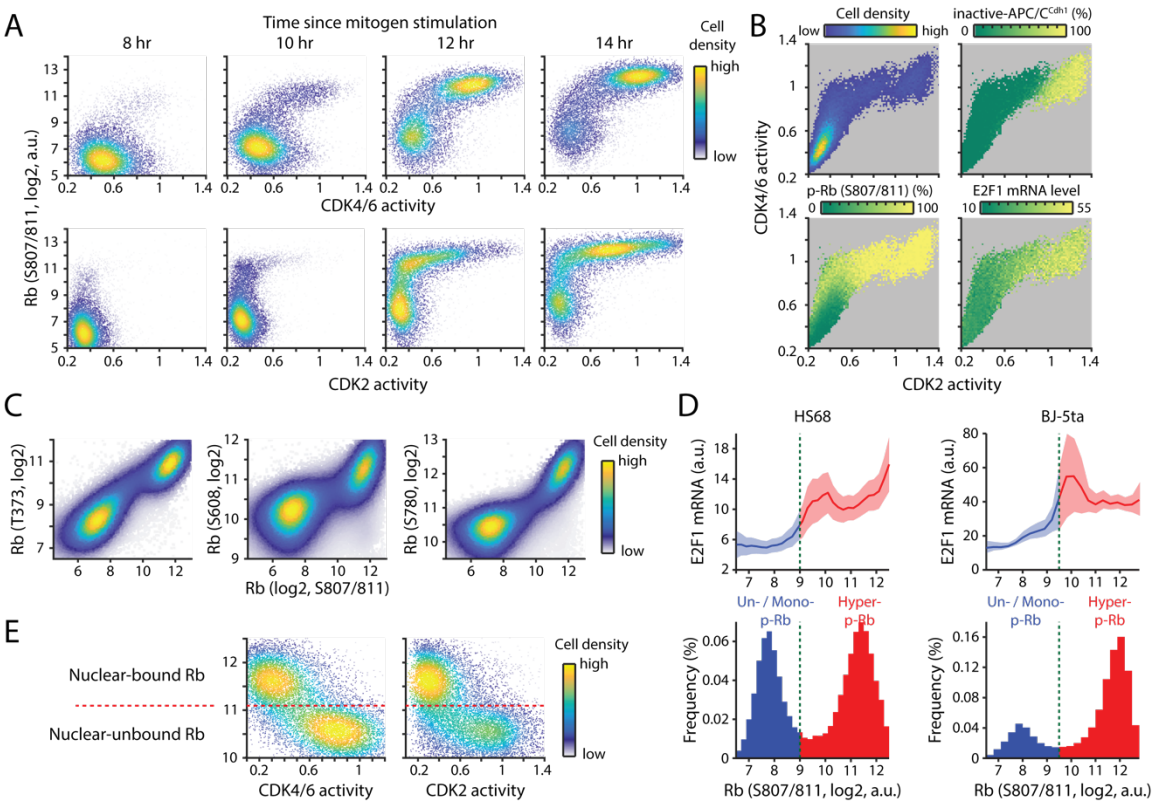

Figure S1. CDK4/6 tightly correlates with Rb phosphorylation and E2F activity before CDK2 activation.

(A) Single-cell correlation of p-Rb at S807/811 versus CDK 4/6 activity (top) and CDK2 activity (bottom) in MCF-10A cells at various time points after mitogen stimulation. Cell density is color-coded. **(B)** Three-dimensional activity map of CDK4/6 versus CDK2 activity in MCF-10A cells where cell density, the percentage of inactivated APC/C^{Cdh1}, the percentage of p-Rb at S807/811, and averaged E2F1 mRNA level are color-coded. **(C)** Left to right, single-cell correlation of Rb phosphorylation at T373, S608, and S780 versus at S807/811. Cell density is color-coded. MCF-10A cells were mitogen-released for 12 hr prior to fixation. **(D)** Top, E2F1 mRNA levels across the distribution of phosphorylated Rb (p-Rb) at S807/811 in HS68 (left) and BJ-5ta (right) cells. Data are mean ± 95% confidence intervals (HS68, n = 158,868 cells; BJ-5ta, n = 92,896 cells). Bottom, histogram of p-Rb at S807/811. Blue and red correspond to un-/mono- and hyper-phosphorylation of Rb, respectively. **(E)** Left, single-cell correlation between nuclear-bound Rb signal and CDK4/6 activity. Right, single-cell correlation between nuclear-bound Rb signal and CDK2 activity. Cell density is color-coded. MCF-10A cells were mitogen-released for 12 hr prior to *in situ* extraction and fixation.

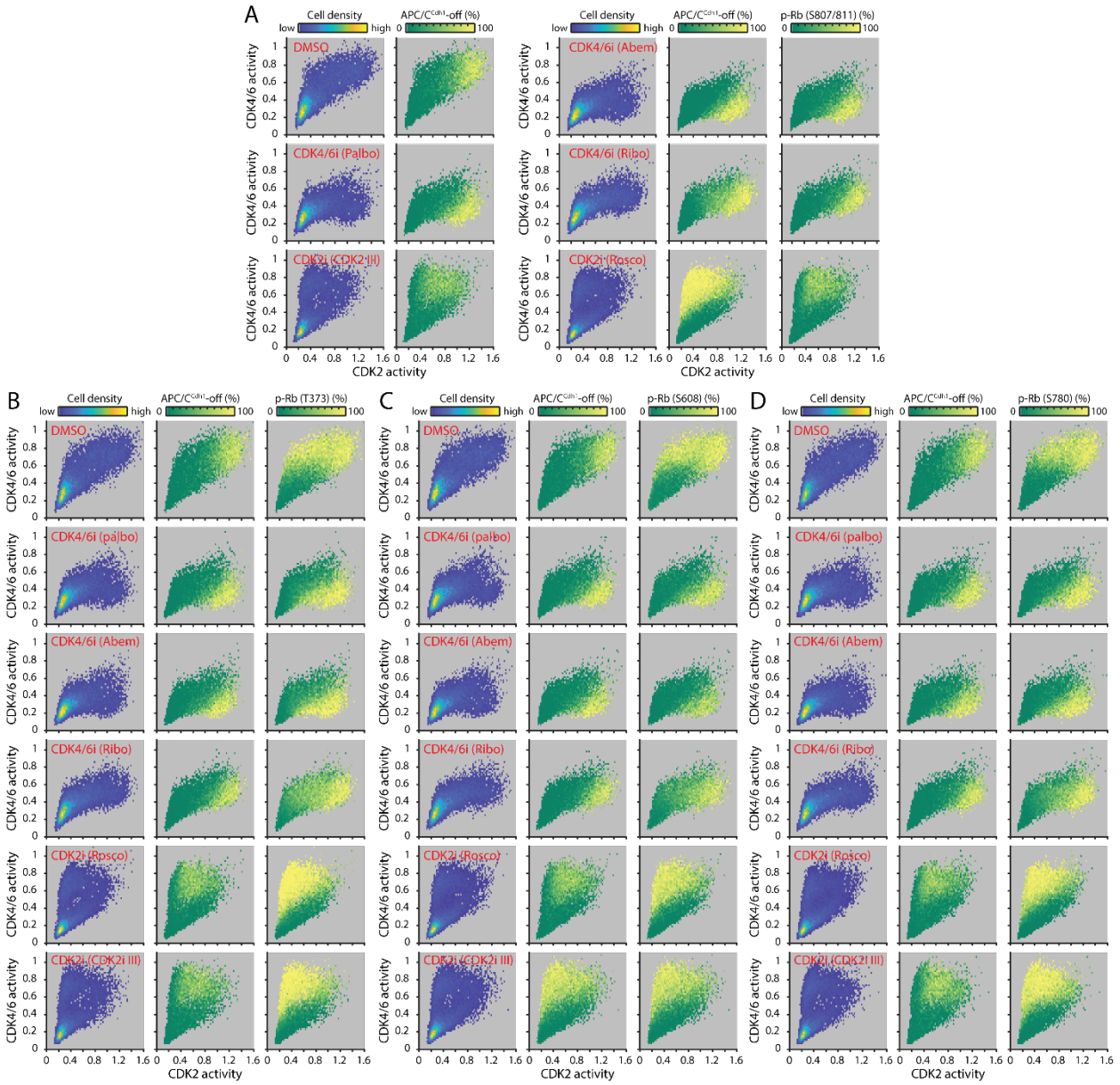

Figure S2. Inhibition of Rb phosphorylation by CDK4/6 inhibitors, but not by CDK2 activation.

(A–D) Three-dimensional activity maps of CDK4/6 versus CDK2 activity under a control condition, CDK4/6 inhibition and CDK2 inhibition. Conditions are color-coded for corresponding cell density, the percentage of inactivated APC/C^{Cdh1}, and the percentage of p-Rb at S807/811 **(A)**, T373 **(B)**, S608 **(C)**, and S780 **(D)**. Maps for the percentage of p-Rb at S807/811 for DMSO, CDK4/6i (palbo), and CDK2i (CDK2i III) are in Figure 2(G). Cells were mitogen-released for 12 hr and treated with DMSO, palbociclib (1 μM), abemaciclib (1 μM), ribociclib (1 μM), roscovitine (60 μM), or CDK2i III (60 μM) for 1 hr prior to fixation.

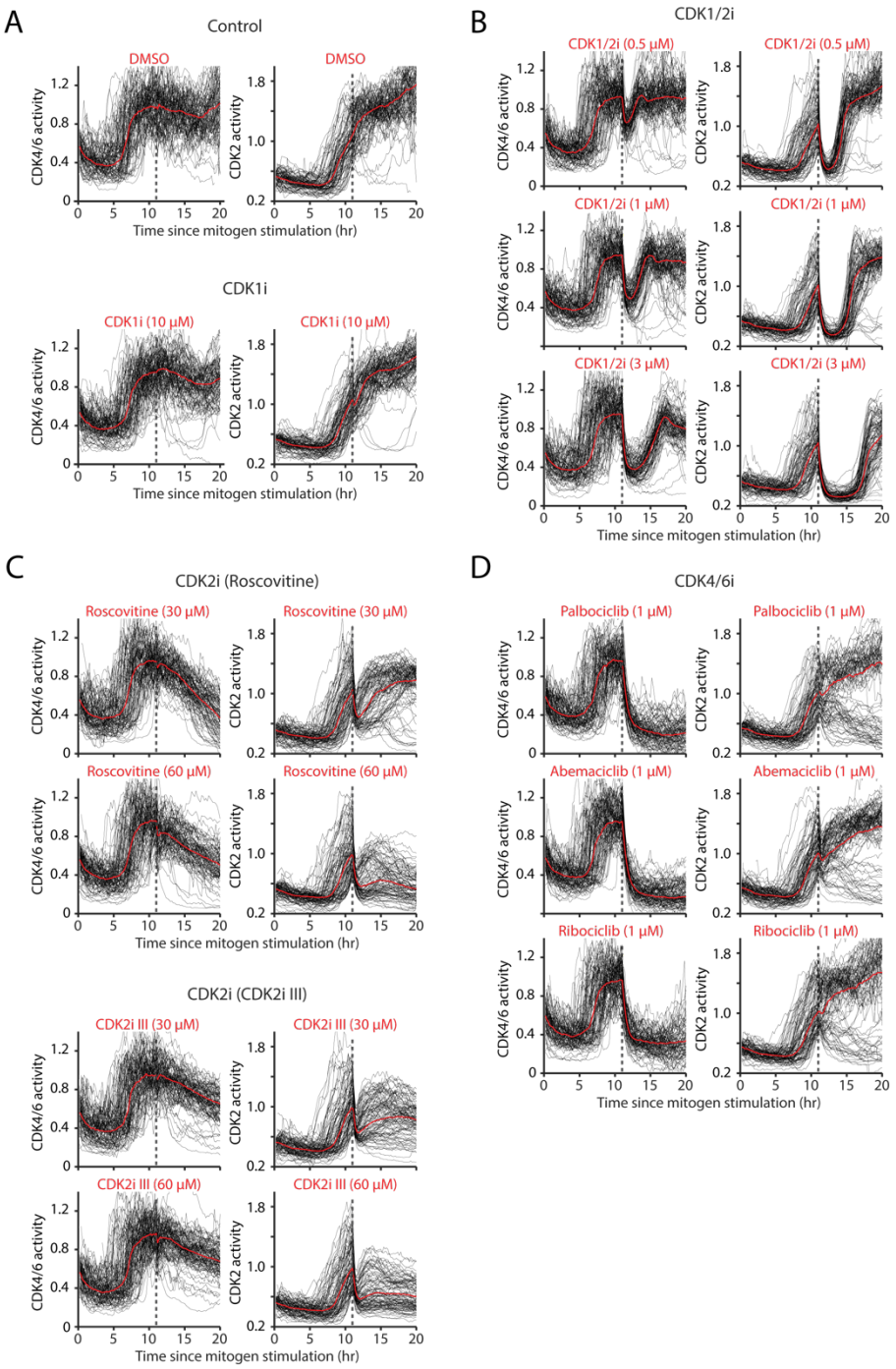

Figure S3. Off-target effects of CDK1/2 and CDK2 inhibitors can suppress not only CDK2 activity, but also CDK4/6 activity.

(A–D) Single-cell traces of CDK4/6 activity (left) and CDK2 activity (right) as a function of time since mitogen release. Cells were mitogen-released for 11 hr, then treated under various conditions. Cells with active CDK4/6 and increasing CDK2 activity were selected based on a threshold of CDK4/6 (> 0.7) or CDK2 (>0.6) at the time of drug treatment. Dotted line indicates time of treatment. **(A)** Top to bottom, control (DMSO) and CDK1 inhibitor (RO-3306, 10 μM). **(B)** Top to bottom, CDK1/2i 0.5 μM, 1 μM, and 3 μM, respectively. **(C)** Corresponding conditions shown for treatment with CDK2 inhibitors. Top, roscovitine 30 μM and 60 μM, respectively. Bottom, CDK2i III 30 μM and 60 μM, respectively. **(D)** Corresponding conditions shown for treatment with CDK4/6 inhibitors. Top to bottom, palbocciclib (1 μM), abemacicclib (1 μM), and ribocciclib (1 μM). Dotted line indicates time of treatment.

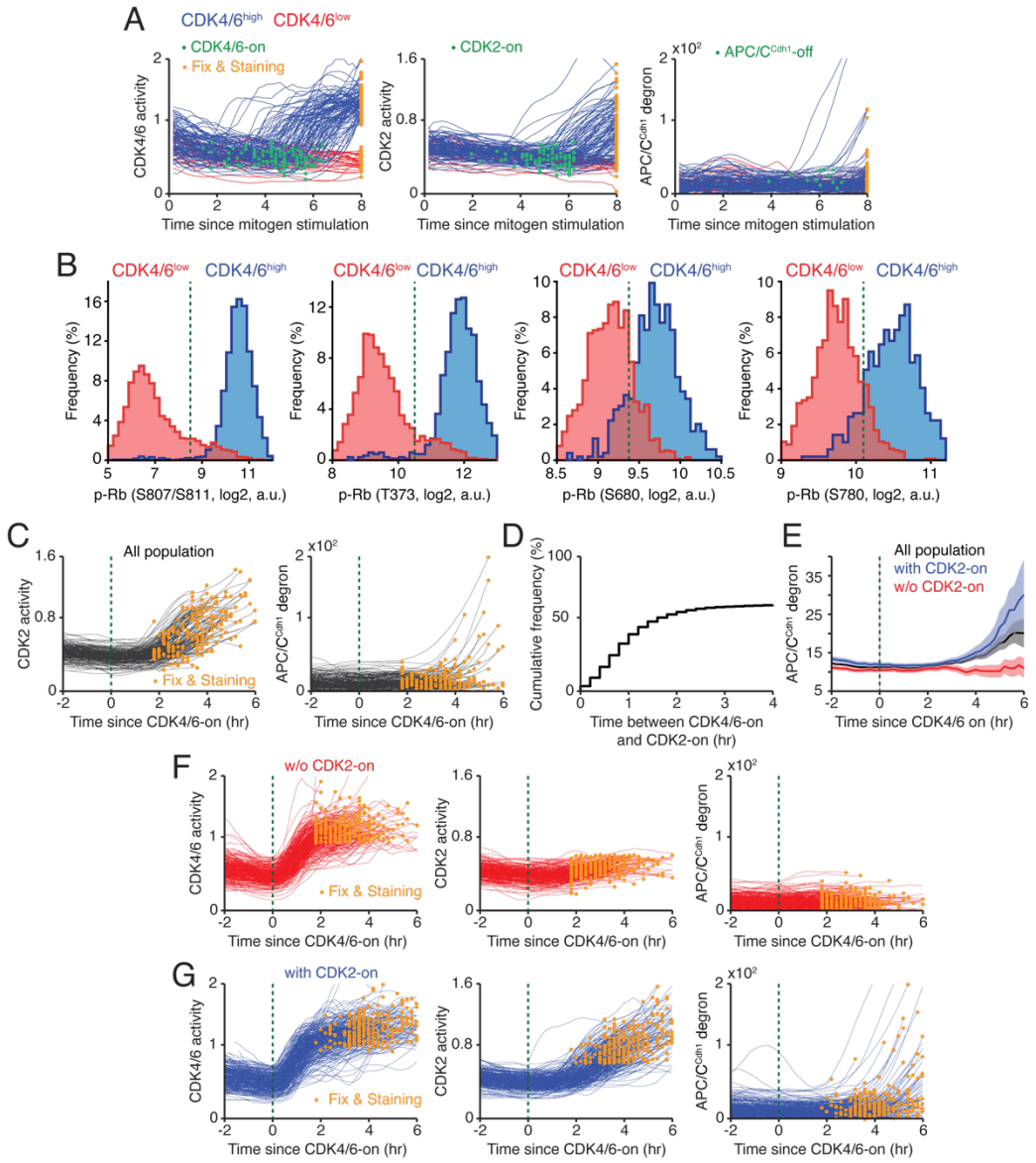

Figure S4. Classification of CDK4/6^{high} cells into populations with or without activated CDK2. **(A)** Left to right, single-cell traces of CDK4/6 activity, CDK2 activity, and APC/C degron for CDK4/6^{high} and CDK4/6^{low} cells as a function of time since mitogen stimulation. Blue and red lines correspond to CDK2^{inc} and CDK2^{low} cells, respectively. Green and yellow points correspond to activation/inactivation point and fixation points, respectively. To create more heterogeneity in the timing of CDK4/6 activation, cells were mitogen-released for various durations (9, 10, and 11 hr) prior to fixation. **(B)** Left to right, distribution of phosphorylated Rb (p-Rb) at S807/811, T373, S608, and S780 for CDK4/6^{low} (red) and CDK4/6^{high} (blue) cells. **(C)** Single-cell traces for CDK2 activity (left) and APC/C degron (right) aligned to the time of CDK4/6 activation in all cell populations. Cells were mitogen-released for various durations (9, 10, and 11 hr) prior to fixation. Yellow point corresponds to fixation point. Green dotted line indicates CDK4/6 activity onset. **(D)** Cumulative frequency of time between CDK4/6 activation and CDK2 activation. **(E)** Averaged APC/C degron traces aligned to CDK4/6 activation. Black, blue, and red lines correspond to all cells, cells with CDK2 activity, and without CDK2 activity, respectively. Green dotted line indicates CDK4/6 activity onset. Data are mean ± 95% confidence interval (All population, n=1,917 cells; with CDK2 activity, n=879 cells; w/o CDK2 activity, n=1,038 cells). **(F)** Left to right, single-cell traces of CDK4/6 activity, CDK2 activity, and APC/C degron aligned to the time of CDK4/6 activation in cells without CDK2 activity. Yellow points correspond to time of fixation. Green

57 dotted line indicates CDK4/6 activity onset. **(G)** Left to right, single-cell traces of CDK4/6 activity,
58 CDK2 activity, and APC/C degron aligned to the time of CDK4/6 activation in cells with CDK2
59 activity. Yellow points correspond to time of fixation. Green dotted line indicates CDK4/6 activity
60 onset.
61

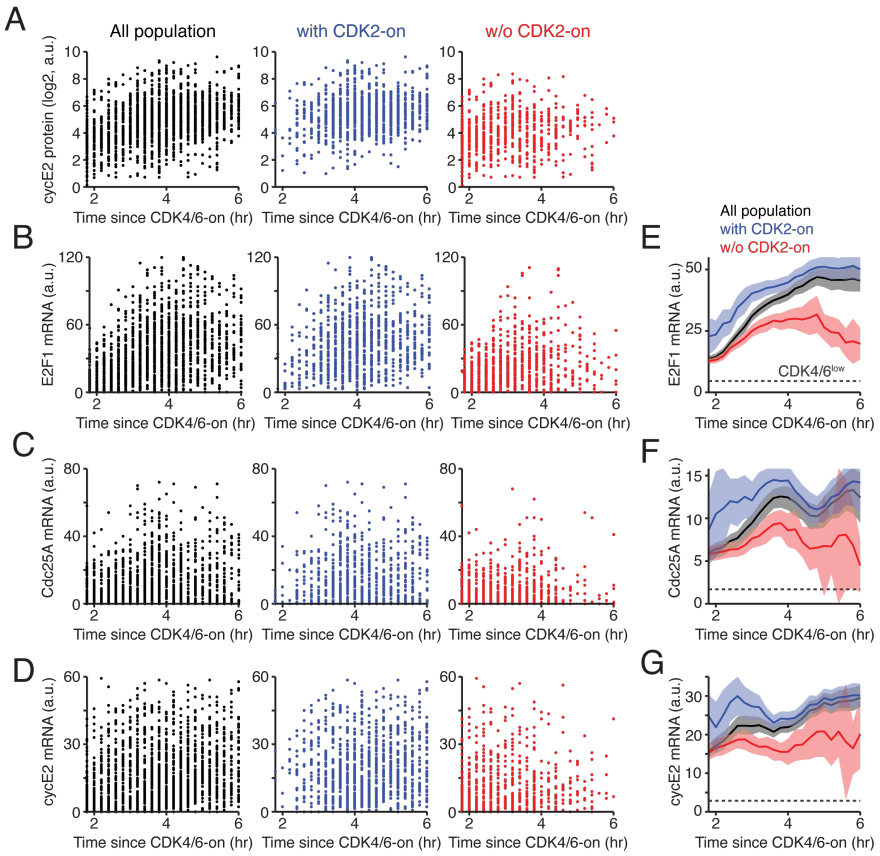

Figure S5. Kinetics of E2F-target gene expression as a function of time since CDK4/6 activation. (A-D) Cyclin E2 protein **(A)**, E2F1 mRNA **(B)**, Cdc25A mRNA **(C)**, and cyclin E2 mRNA **(D)** levels versus time since CDK4/6 activation. Left to right, all cell populations (black), cell population with CDK2 activity (blue) and without CDK2 activity (red). **(E-G)**, Averaged E2F1 mRNA **(E)**, Cdc25A mRNA **(F)**, and cyclin E2 mRNA **(G)** levels aligned to the time of CDK4/6 activation. Black, blue, and red lines correspond to all cells, cells with CDK2 activity, and without CDK2 activity, respectively. **(E)** Dotted line indicates E2F1 mRNA level in CDK4/6^{low} cells. Data are mean ± 95% confidence interval (All population, n=1,917 cells; with CDK2 activity, n=1,038 cells; w/o CDK2 activity, n=879 cells; CDK4/6^{low} cells, n=4,493 cells). **(F)** Dotted line indicates Cdc25A mRNA level in CDK4/6^{low} cells. Data are mean ± 95% confidence interval (All population, n=1,981 cells; with CDK2 activity, n=1,068 cells; w/o CDK2 activity, n=913 cells; CDK4/6^{low} cells, n=4,462 cells). **(G)** Dotted line indicates Cdc25A mRNA level in CDK4/6^{low} cells. Data are mean ± 95% confidence interval (All population, n=1,930 cells; with CDK2 activity, n=1,226 cells; w/o CDK2 activity, n=704 cells; CDK4/6^{low} cells, n=3,986 cells).

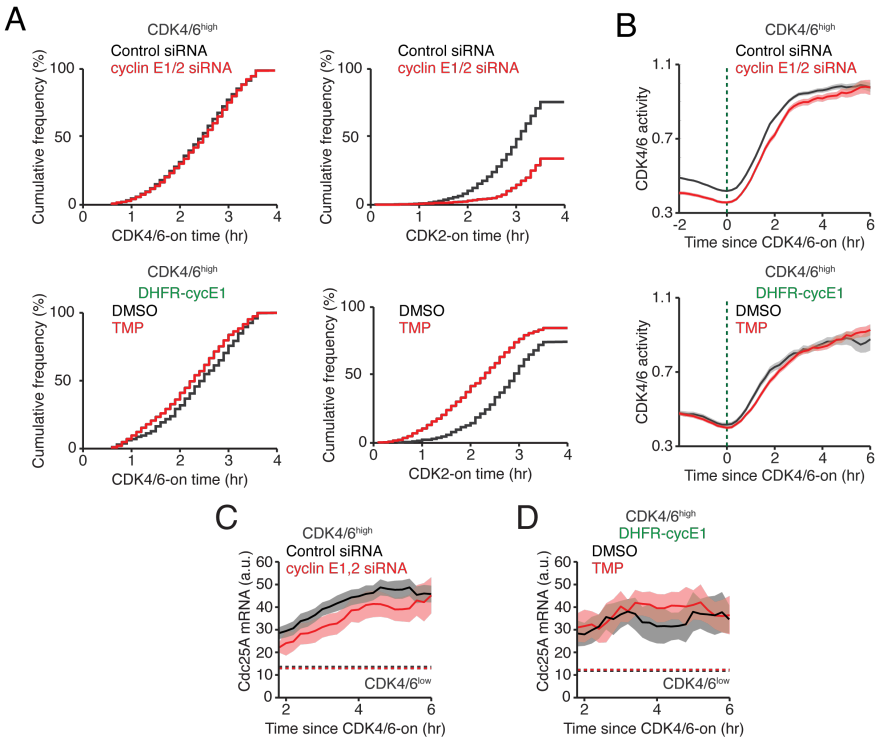

Figure S6. CDK4/6 activation triggers full activation of E2F activity without CDK2 activity. **(A,B)** Cumulative frequency of cells with CDK4/6 activation (left) and CDK2 activation (right) in CDK4/6^{high} cells **(A)**. Average CDK4/6 activity traces aligned to the time of CDK4/6 activation in CDK4/6^{high} cells **(B)**. Green dotted line indicates CDK4/6 activity onset **(B)**. Top, MCF-10A cells were treated with control (black) and cyclin E1/2 siRNA. Bottom, MCF-10A cells expressing DHFR-cyclin E1 were mitogen-released without (black) or with (red) TMP (50 µM). Data are mean ± 95% confidence interval (Cells treated with control siRNA, n=3,172 cells; cyclin E1/2 siRNA, n=1,042 cells; DMSO, n=470 cells; TMP n=932cells). **(C,D)** Averaged Cdc25A mRNA levels aligned to the time of CDK4/6 activation for CDK4/6^{high} cells. Dotted line indicates Cdc25A mRNA level in CDK4/6^{low} cells. MCF-10A cells were transfected with control (black) or cyclin E1/2 (red) siRNA and were mitogen-released for various durations (9, 10, and 11 hr) prior to fixation **(C)**. MCF-10A cells expressing DHFR-cyclin E1 were mitogen-released for various durations (9, 10, and 11 hr) with DMSO (black) or TMP (50 µM, red) prior to fixation **(D)**. Data are mean ± 95% confidence interval (c, siRNA: Control, n=387 cells; cyclin E1/2, n=921 cells; d, DHFR-cyclin E1: DMSO, n=574 cells; TMP, n=495 cells).

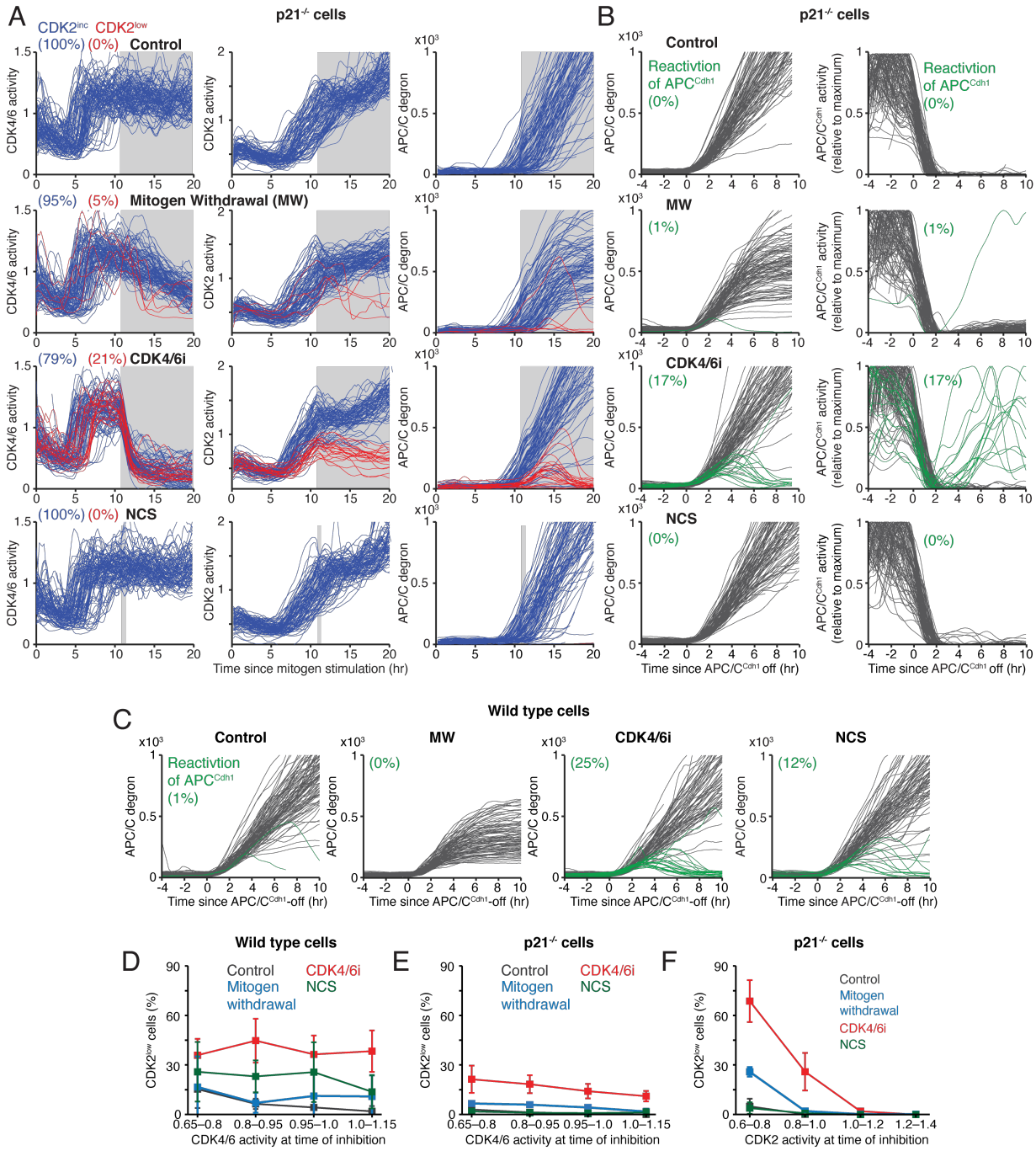

Figure S7. CDK2 activity determines the commitment point in cell-cycle entry.
(A) Single cell traces of CDK4/6 activity (left), CDK2 activity (middle), and APC/C degron (right) in p21 knockout cells with corresponding treatment conditions shown for control, CDK4/6 inhibitor (palbociclib, 1 μM), mitogen withdrawal, and 10 min NCS pulse (100 ng/ml) (top to bottom). All treatments performed at 11 hr (marked in gray). Blue and red lines correspond to $CDK2^{inc}$ and $CDK2^{low}$ cells, respectively. **(B,C)** Single-cell traces of APC/C degron (left) and APC/C^{Cdh1} activity (right) in p21 knockout cells **(B)** and wild type cells **(C)** aligned to the time of APC/C^{Cdh1} inactivation under treatment conditions in **(A)**. Gray and green lines correspond to cells maintaining APC/C^{Cdh1} inactivation and cells reactivating APC/C^{Cdh1}, respectively. **(D,E)** Percentage of $CDK2^{low}$ cells in wild type cells **(D)** and p21 knockout cells **(E)** for each treatment condition in **(A)**.

Cells were classified based on CDK4/6 activity at the time of inhibition. Data are mean ± s.d. (n = 3 biological replicates). **(F)** Percentage of $CDK2^{low}$ cells for increasing levels of CDK2 activity at the time of inhibition, in p21 knockout cells. Cells were classified based on each treatment condition in **(A)**. Data are mean ± s.d. (n = 3 biological replicates).

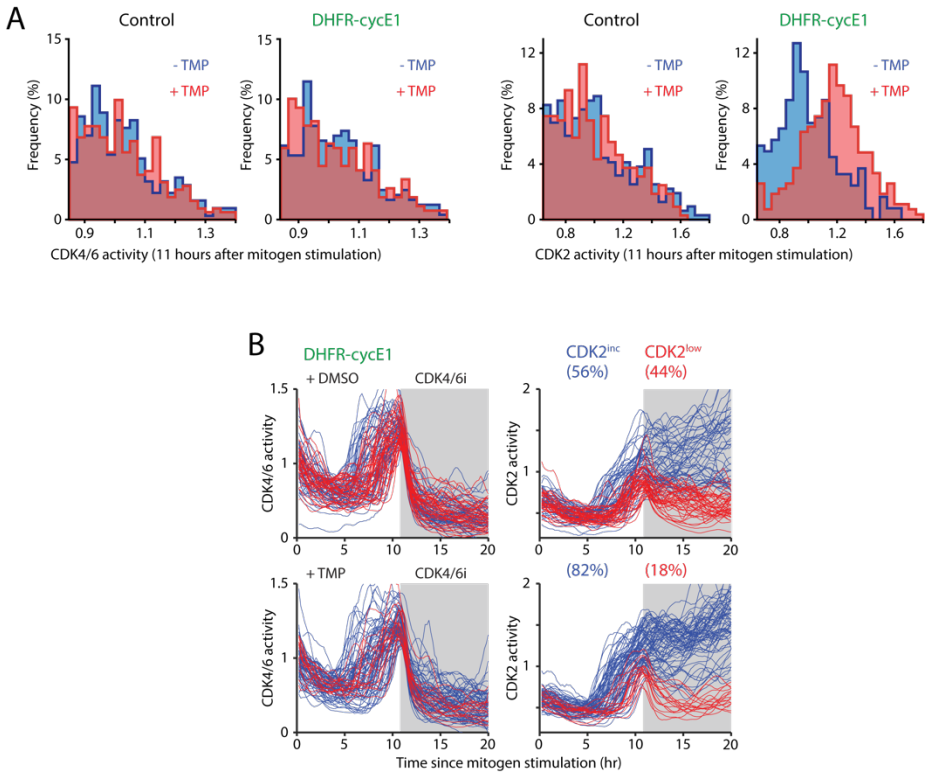

Figure S8. Regulation of CDK2 activity determines the restriction point.
(A) Distribution of CDK4/6 activity (left) and CDK2 activity (right) for control (black) and DHFR-cyclin E1 (green) cells 11 hr after mitogen stimulation. Red and blue indicate cells with and without the addition of TMP (50 μM), respectively. **(B)** Single-cell traces of CDK4/6 activity (left) and CDK2 activity (right). MCF-10A cells expressing DHFR-cyclin E1 were mitogen-released without (top) or with (bottom) TMP (50 μM). CDK4/6 inhibitor (palbociclib, 1 μM) was added 11 hr after mitogen stimulation. Blue and red lines correspond to $CDK2^{inc}$ and $CDK2^{low}$ cells, respectively.

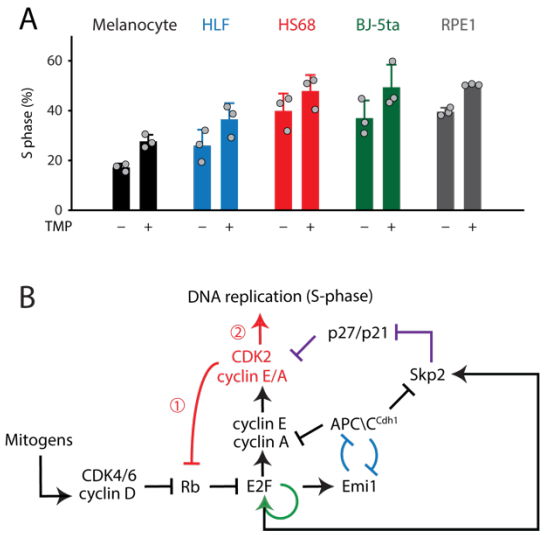

Figure S9. CDK2 activity level regulates S-phase entry.
(A) Percentage of cells in S phase for Melanocyte (black), HLF (blue), HS68 (red), BJ-5ta (green), and RPE1 (gray) cells with or without TMP (50 μM). Cycling cells were treated with or without TMP for 6 hr followed by treatment with EdU (10 μM) for 15 min prior to fixation. Data are mean ± s.d. (n = 3 biological replicates). **(B)** Schematic of the regulation of the Rb/E2F pathway.